The Journal of Chemical Physics

Development and initial applications of an e-ReaxFF description of Ag nanoclusters

Benjamin Evangelisti[1], Kristen A. Fichthorn[2,4] and Adri C. T. van Duin[1,2,3]

Email: acv13@psu.edu

[1]: Department of Chemistry, Pennsylvania State University, University Park, Pennsylvania 16802, USA.

[2]: Department of Chemical Engineering, Pennsylvania State University, University Park, Pennsylvania 16802, USA.

[3]: Department of Mechanical Engineering, Pennsylvania State University, University Park, Pennsylvania 16802, USA.

[4]: Department of Physics, Pennsylvania State University, University Park, Pennsylvania 16802, USA.

The Journal of Chemical Physics

Abstract

Metal nanocrystals are of considerable scientific interest because of their uses in electronics, catalysis, and spectroscopy, but the mechanisms by which nanocrystals nucleate and grow to achieve selective shapes are poorly understood. *Ab initio* calculations and experiments have consistently shown that the lowest energy isomers for small silver nanoparticles exhibit two-dimensional (2D) configurations and that a transition into three-dimensional (3D) configurations occurs with the addition of only a few atoms. We parameterized an e-ReaxFF potential for Ag nanoclusters ($N \leq 20$ atoms) that accurately reproduces the 2D-3D transition observed between the Ag_5 and Ag_7 clusters. This potential includes a four-body dihedral term that imposes an energetic penalty to 3D structures that is significant for small clusters, but is overpowered by the bond energy from out-of-plane Ag-Ag bonds in larger 3D clusters. The potential was fit to data taken from density-functional theory and coupled-cluster calculations and compared to an embedded atom method potential to gauge its quality. We also demonstrate the potential of e-ReaxFF to model redox reactions in silver halides and plasmon motion using molecular dynamics simulations. This is the first case in which e-ReaxFF is used to describe metals. Furthermore, the inclusion of a bond-order dependent dihedral angle in this force field is a unique solution to modelling the 2D-3D transition seen in small metal nanoclusters.

Introduction

Silver metal nanocrystal growth is an active field of research due to the many applications of these crystals in electronics[1–5], imaging[6,7], and catalysis[8,9] that result from their unique optical and electronic properties. The structure of a crystal often dictates its properties and much progress has been made in shape-selective crystal growth, albeit with a relatively poor understanding of the growth mechanisms themselves[5,10–13]. The smallest silver nanoclusters (N < 7 atoms) are fascinating because *ab initio* calculations and spectroscopic studies predict that their preferred structures are two-dimensional (2D) while larger clusters prefer a three-dimensional (3D) geometry[14–18]. In their exhaustive study comparing 42 different exchange-correlation functionals to high-level *ab initio* calculations and experiments, Duanmu *et al.* found that many of the 3D local minima for clusters with 5 or 6 atoms are several kcal/mol higher in energy than any corresponding 2D isomer, while 2D 7-atom clusters are several kcal/mol higher in energy than many 3D isomers[16]. Aggregation involving these 2D clusters may be responsible for structure-determining phenomena in larger crystals, such as stacking faults and twinning.

Nanocrystal growth occurs over timespans ranging from seconds to hours, with Ag clusters 2-3 nm in size being produced within seconds of reagent mixing in experiment[19,20]. Modelling the dynamics of a crystal of that size or larger is intractable with *ab initio* methods. Empirical force-field based molecular dynamics (MD) methods can model larger systems over much longer timespans than *ab initio* methods, making them better suited for the study of processes involved in nanocluster synthesis.

Metal nanoclusters grow from salt feedstocks via a complex series of intermediates that vary in size, connectivity, and net charge. These aspects of cluster growth limit the applicability of many traditional MD methods, which are non-reactive. The ReaxFF reactive force field

method[21] has been used to describe a variety of different chemical systems such as metal surface chemistry[22,23], hydrocarbon combustion[24], and solid-liquid interfaces[22,25–27]. A recent extension to this method, termed e-ReaxFF, introduced an explicit electronic degree of freedom into ReaxFF, allowing for the modelling of redox processes, in addition to the systems already covered by ReaxFF[28]. In this paper, we introduce an e-ReaxFF force field designed to reproduce the structure of Ag nanoclusters.

This paper will briefly describe the e-ReaxFF method, our force field training and parameterization methods, and the resulting force field's ability to reproduce density functional theory (DFT) and coupled cluster (CCSD(T)) data for Ag nanocluster isomer energy differences. We subsequently demonstrate that our potential can describe structural transitions in Ag clusters based on cluster size, can capture oxidation state changes for halide reactions with Ag-cations, and can model plasmon resonance.

Methods

Molecular Dynamics Simulations

Unless otherwise noted, all MD simulations were conducted using the standalone ReaxFF code in the canonical (NVT) ensemble using the Nose-Hoover thermostat to maintain a constant temperature. A timestep of 0.250 fs was used to account for the fast movements of the explicit electrons. Neutral silver atoms are represented by an Ag^+ cation and an electron (silver sphere and green spheres in figures, respectively).

e-ReaxFF

ReaxFF is a general bond order (BO) based classical force field method that allows for on-the-fly bond breaking and formation during MD simulations[21]. In the e-ReaxFF model, an explicit electron is introduced into ReaxFF as an additional pseudoclassical particle with a -1

charge which is paired with a +1 charged cation in neutral systems. e-ReaxFF required modifications to several of the ReaxFF partial energy terms to account for this change, but the general components of the original potential energy function were retained. The potential energy in e-ReaxFF is given by

$$E_{system} = E_{bond} + E_{over} + E_{under} + E_{lp} + E_{val} + E_{tor} + E_{vdWaals} + E_{Coulomb} + E_{nucl} + E_{el} \quad (1)$$

where the partial energy contributions (indicated by corresponding subscripts) include bond, over-coordination penalty and under-coordination stability, lone pair, valence, torsion, as well as non-bonded van der Waals, Coulomb, and nucleus-electron interaction contributions.

The two-body (bond), three-body (valence angle), and four-body (torsional) interaction functional forms used in standard ReaxFF[21] are retained in e-ReaxFF with changes made to the over-coordination penalty, under-coordination stability, and lone pair terms accounting for the inclusion of explicit electrons. Additionally, electron-electron and electron-nuclei interactions were also added with the addition of the explicit electron. The non-bonding van der Waals and Coulombic interactions are unchanged from those used in ReaxFF. e-ReaxFF uses the atom-condensed Kohn-Sham approximated to the second order (ACKS2)[29] charge calculation scheme instead of the electronegativity equalization method (EEM)[30] used by most ReaxFF potentials.

The presence of an explicit electron near a nucleus changes the number of valence electrons of this nucleus (*e.g.* C, which normally has 4 valence electrons, reduces its number of valence electrons to 3 when it is in the vicinity of an explicit electron). In the case of silver, at least one electron needs to be paired with an Ag^+ cation so that a valency of 1 is achieved and a neutral Ag atom is formed. Ag-Ag bonds only form when at least one of the two Ag atoms is neutral since an Ag^+-Ag^+ bond is de-stabilized by its over-coordination penalty. These changes to the atom

valency, which couple to the over-coordination term, are necessary to connect an atom's charge to its valency; this connection is absent in standard ReaxFF.

The e-ReaxFF method has been used previously to describe hydrocarbons[28]. However, in that case there was only one electron associated with a molecule, while the model for silver presented here describes every neutral silver atom as a positive Ag^+ cation paired with an electron in a quasi-Drude fashion. e-ReaxFF currently uses a mass of 1 amu for an electron to facilitate taking timesteps that are large enough to enable tractable nanosecond MD simulation times. Because the number of electrons around a silver atom is not fixed, an exponential function centered on the atom is used to calculate its number of associated electrons. In this way, one can model a partial delocalization. The exponential function is of the form

$$n_{el} = \exp\left(-p_{val} \cdot R_{ij}^2\right) \quad (2)$$

where R_{ij} is the distance between the atom-center and the electron and p_{val} is a general parameter in the force field.

Force Field Training

The accuracy of an MD simulation highly depends on the ability of the force field to reproduce the potential-energy landscape of the specified system. We trained our e-ReaxFF force field using the standalone e-ReaxFF code to reproduce the energy differences between different Ag isomers for cluster sizes from *N* = 2-7 atoms and with net charges of +1, 0, and -1 taken from the DFT study of Duanmu *et al*. [16] These structures and their corresponding energies were obtained using CCSD(T) calculations.[31] In addition, we included (with lower weight) the lowest-energy isomer for cluster sizes ranging from *N* = 2-20 atoms from the study of Chen *et al.*, [32] who used DFT calculations based on the B3LYP exchange functional[33,34] and the aug-cc-pVDZ-PP basis set[35].

In addition to isomer energy differences, our training set included electron affinities, ionization energies, and cohesive energies. In e-ReaxFF, the electron affinity is defined as

$$EA(X) = E_x - E_x^- \tag{3}$$

where E_X and E_X^- are the energy of a species in a neutral state and in a state with an additional electron respectively, and E_{el} is the energy of an electron. The ionization energy in e-ReaxFF is similarly defined as

$$IE(X) = E_x^+ - E_x \tag{4}$$

where E_X^+ is the energy of a species in a state with one fewer electron and the other terms remaining the same. The cohesive energy in e-ReaxFF is defined as

$$CE(N) = E_1 - {}^{E_N}/_N \tag{5}$$

where E_N is the energy of the lowest energy isomer with N atoms and E_1 is the energy of a single atom.

Parameter optimization was conducted using a successive one-parameter search technique to minimize the following expression for the error

$$error = \sum_i^n \left[\frac{(x_{i,lit} - x_{i,eReaxFF})}{\sigma_i}\right]^2 \tag{6}$$

where x_{lit} is the target value – in this case the DFT or CCSD(T) value – for the energy difference between the most-stable isomer and isomer i, $x_{eReaxFF}$ is the e-ReaxFF value for this energy difference, and σ_i is the weight assigned to data point i.

Silver Torsional Terms

We initially assumed that a description for silver would only require one-body and two-body (atom and bonding) terms to be parameterized to reproduce DFT energies. This assumption was made for two primary reasons: ReaxFF has been used to describe *bulk* metals in the past[36] using

only these terms and the inclusion of three-body and four-body terms necessarily increases the computational cost of the force field. Our initial goal for this force field was to replicate the 2D-3D transition observed between the lowest-energy isomers for Ag_5 and Ag_7 clusters. However, we were unable to replicate this phenomenon while maintaining a positive cohesive energy. We opted to include three-body and four-body angular and torsional terms, respectively, in our parameter optimization because torsional terms have established usage in describing 2D molecules such as graphene.[37] The three-body term was only included because e-ReaxFF requires a three-body description to recognize a four-body interaction.

The physical justification behind including a dihedral term in a metal description is somewhat uncertain, but we believe that we are reproducing the effects of quasi-sd^4 orbital hybridization which are suspected to be the cause of 2D nanoclusters in transition metals.[38] Most of the work performed in this area has been on Au, which shows stable 2D clusters into the low-teens of atoms in size.[39,40] For Au, this 2D preference for enhanced sizes is the result of relativistic effects that enhance quasi-sd^4 hybridization significantly more than what is encountered in Ag nanoclusters.[41] By including a dihedral term in the e-ReaxFF, we mimic this effect.

Figure 1 shows the torsion potential energy and the sum of the bond and over-coordination potential energies during MD simulations of the transformation of a 2D Ag_{25} sheet to a 3D Ag_{25} cluster. The Ag_{25} sheet actively collapsed into a 3D cluster because the bonding term heavily outweighs the torsional penalty for breaking planarity. In Figure 1, the over-coordination term is included with the bonding term from Eq.(1) because changes in the connectivity of a structure when going from 2D to 3D directly influence changes in the over-coordination penalty. If this

term was absent in Figure 1, the bonding potential energy term would be much larger and would imply a greater stability than what is actually observed.

As seen in Figure 1, the dihedral terms are parameterized such that the torsion potential energy [E_{tor} in Eq. (1)] is zero for 2D structures and positive for 3D structures. The torsion potential is balanced by the bonding and over-coordination potentials such that large clusters collapse into 3D structures while small clusters flatten out in 2D.

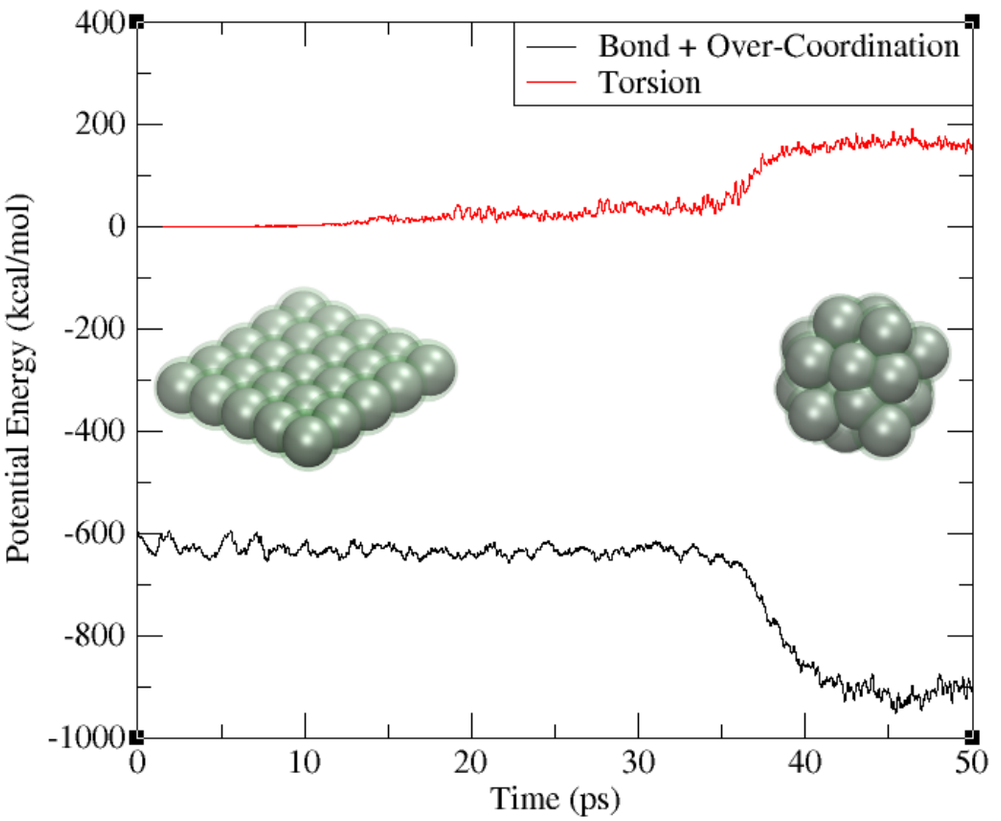

Figure 1. Torsion potential energy [E_{tor} in Eq. (1)] during an MD simulation of a 2D Ag_{25} sheet at T = 500 K. While the cluster remains planar, the torsion potential energy is zero. As the cluster collapses into a 3D structure, the torsion potential energy increases and is compensated for by a decrease in the bonding and over-coordination energies [E_{bond} and E_{over} in Eq. (1)].

Results and Discussion

Force Field Fitting

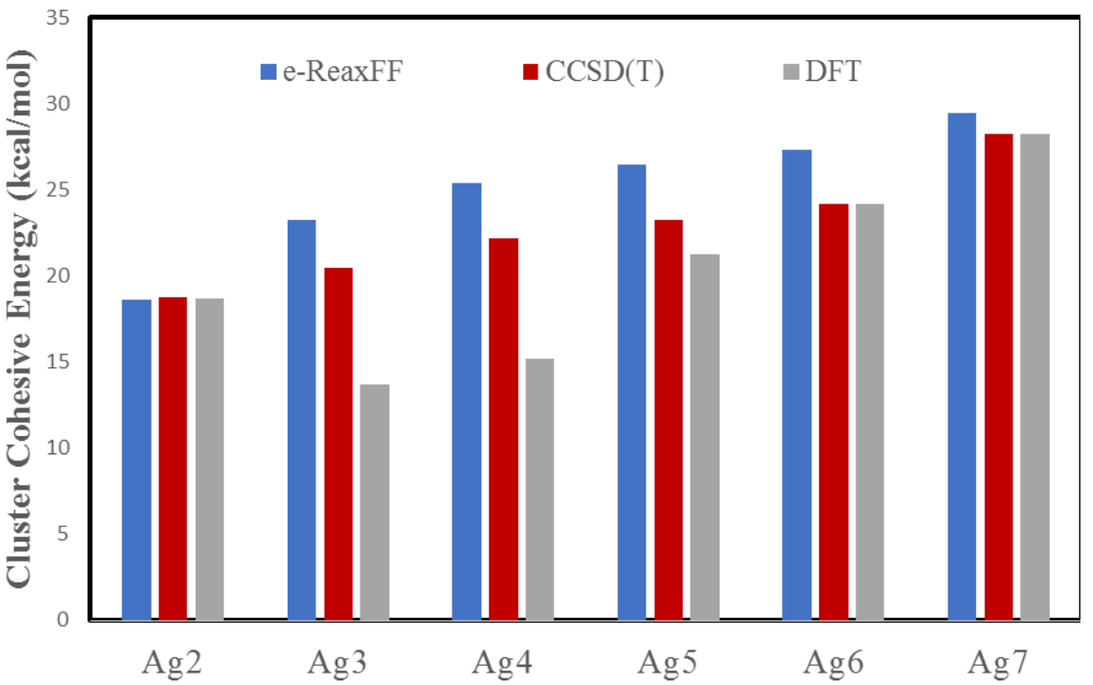

Figure 2. Cohesive energies [Eq. (6)] of Ag_2 to Ag_7 calculated with e-ReaxFF, CCSD(T)[16], and DFT[32].

Figure 2 shows the cohesive energy, given by Eq. (6), as a function of cluster size for the lowest-energy isomers of clusters ranging in size from N = 2-7 in comparison to DFT energies from the study of Chen *et al.*[32] and CCSD(T) energies from the study of Duanmu *et al*[16]. We note that there is an appreciable disagreement between the DFT and CCSD cohesive energy values for Ag_3, Ag_4, and Ag_5. The CCSD(T) values are more accurate than DFT values and are taken as the standard of comparison for these cluster sizes. We see that e-ReaxFF shows better agreement with the CCSD(T) cohesive energies than the DFT calculations for these structures – although e-

ReaxFF overestimates the cohesive energies for Ag_3 to Ag_6 by approximately 13%. e-ReaxFF shows excellent agreement with both methods for Ag_2 and good agreement with both methods for Ag_7.

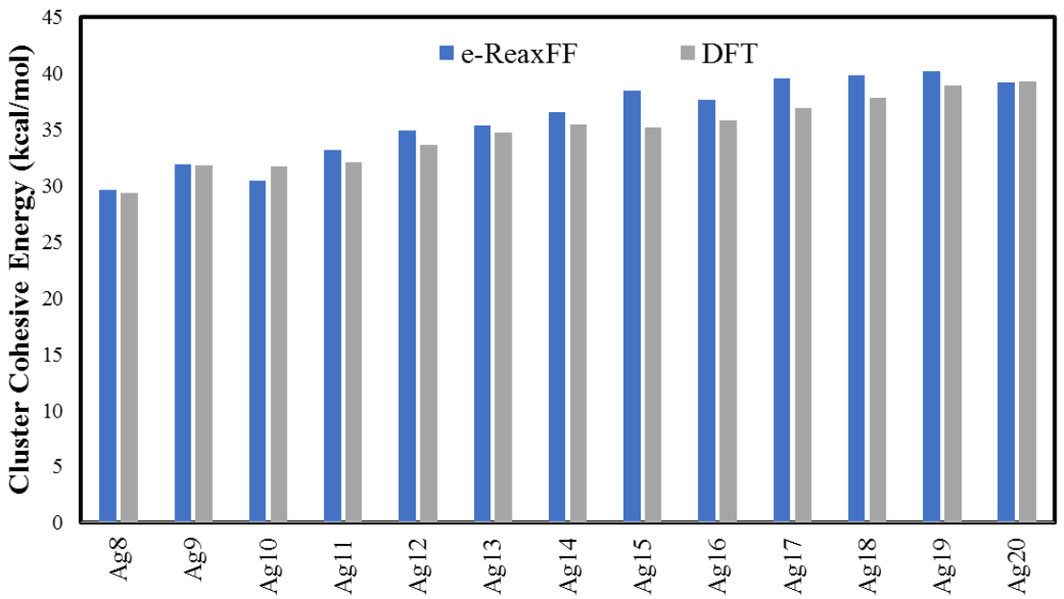

Figure 3. Cohesive energies [Eq. (6)] of Ag_8 to Ag_{20} calculated with e-ReaxFF and DFT[32].

Figure 3 shows the cohesive energy, given by Eq. (6), as a function of cluster size for the lowest-energy isomers of clusters ranging in size from N = 8-20 in comparison to DFT energies taken from Chen *et al*.[32] Here, we see that e-ReaxFF shows good agreement with the DFT cohesive energies, with errors of 5% or less for all structures except Ag_{15}. e-ReaxFF overestimates the cohesive energy of Ag_{15} by 9%, which is most likely due to the cage-like portion of its structure noticeably contracting during energy minimization compared to the DFT structure.

Duanmu *et al.*[16] tested a considerable number of neutral and charged Ag_5, Ag_6, and Ag_7 isomers that we included in our training set. In total, there were 127 unique structures for these three cluster sizes with net charges of -1, 0, or +1. Many of these structures, however, do not contribute significantly to a partition function at typical MD and experimental temperatures. Of particular importance to us was producing a force field that can correctly determine whether an Ag nanocluster will be most stable as a 2D or 3D cluster.

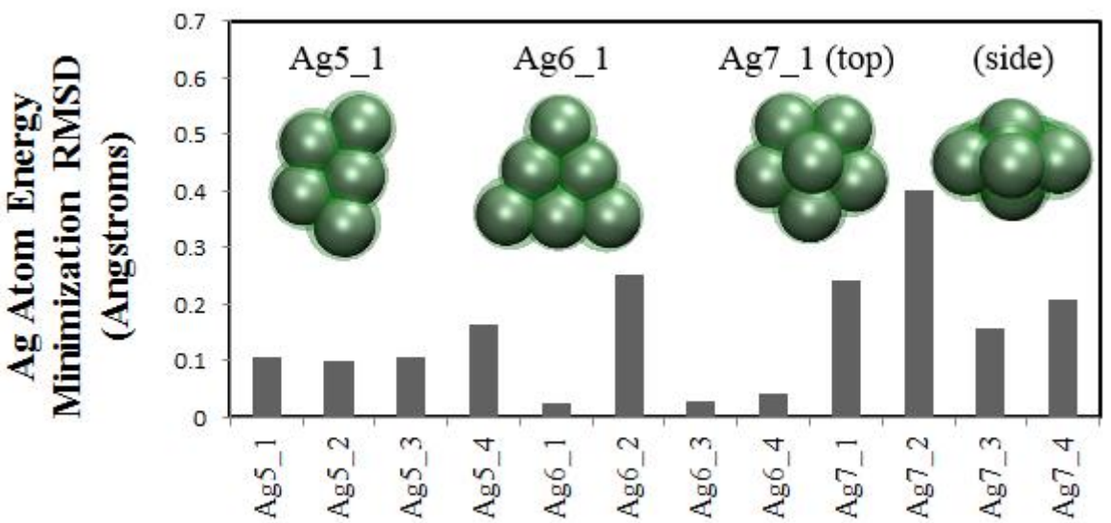

Figure 4. Ag atom RMSD values between the CCSD(T) structures calculated by Duanmu *et al*[16]. and the energy minimized e-ReaxFF structures for the first four Ag_5, Ag_6, and Ag_7 isomers in our training set.

We calculated the root-mean-square deviation (RMSD) of the Ag atomic coordinates for all of the Ag_5-Ag_7 clusters between the CCSD(T) coordinates and the coordinates following energy minimization with e-ReaxFF in order to quantify the structural deviation between methods. Figure 4 includes the RMSD for the four-lowest energy isomers for these cluster sizes. The structures in Figure 4 are indexed as Ag*N*_*x*, in which *N* is the number of atoms in the cluster and *x* is the energetic ranking of the geometry with regard to the lowest-energy cluster of that size

(*e.g.* Ag5_1 is the Ag_5 isomer with the lowest energy and Ag5_4 is the Ag_5 isomer with the fourth-lowest energy). Larger RMSD values were observed for 3D structures than for 2D structures because the dihedral term slightly disturbs the equilibrium bond length in non-planar geometries, but no RMSD exceeded 1.0 Angstroms following energy minimization. Of particular importance was that the lowest energy isomers show low RMSDs because we often used these structures as reference energies during the parameter optimization.

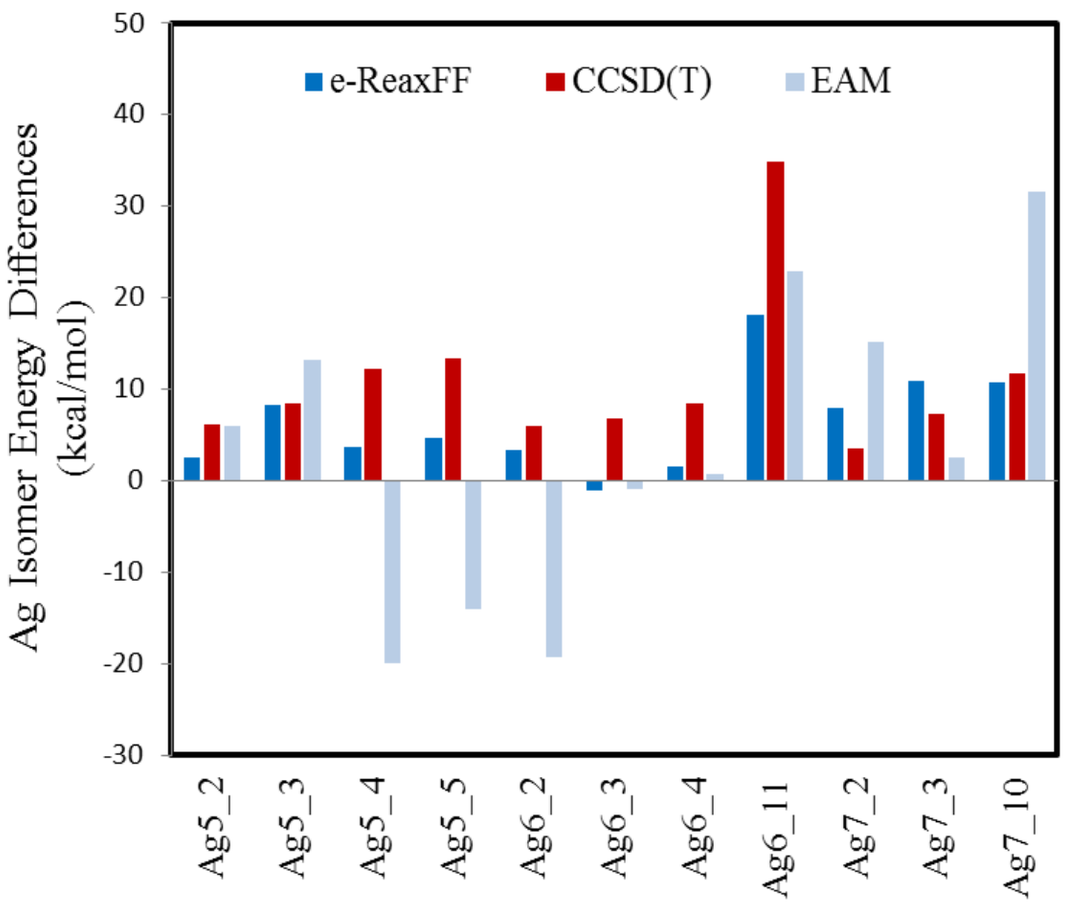

Figure 5. Ag cluster isomer energy differences calculated using e-ReaxFF and the EAM potential of Williams *et al.*[42] in comparison to results from the CCSD(T) calculations of Duanmu *et al.*[16]

In Figure 5, we present Ag cluster energies relative to the lowest-energy isomer for a given size for e-ReaxFF, the embedded-atom method (EAM) potential of Williams *et al.*[42], and the CCSD(T) calculations of Duanmu *et al.*[16] We included an EAM potential because these potentials have low computational cost and high accuracy for bulk metals and their low-index surfaces, making them widely used. The structures in Figure 5 give a general overview of the key and not-so-key structures included in the data set. Of most importance among the neutral clusters are Ag5_4, Ag5_5, Ag6_2, and Ag7_10; these structures, with the exception of Ag7_10, are all 3D structures while their most-stable isomer is 2D. Ag7_10 is the reverse and is a 2D isomer of the typically 3D Ag_7.

In Figure 5, we see that the EAM potential significantly over-stabilizes 3D isomers of Ag_5 and Ag_6. The magnitude of this over-stabilization is such that any cluster with four or more atoms will be 3D. This is primarily because EAM lacks a dihedral term in its potential that can stabilize 2D geometries and instead it seeks to maximize the number of bonds in the system, an important trait of bulk metals, but unrealistic at the cluster scale. However, e-ReaxFF was fitted such that Ag5_1 and Ag7_1 are both the most-stable structure for their respective cluster sizes while also correctly determining the 2D structure of Ag_4. This is because its torsion potential energy term penalizes all 3D structures, but below Ag_7, there are not enough bonds to resist converting from 3D to 2D. Ag6_3 has a slight energetic preference over Ag6_1 in e-ReaxFF, which disagrees with the *ab initio* calculations. However, both Ag6_1 and Ag6_3 are 2D structures which preserve the planarity of Ag_6 with the e-ReaxFF method.

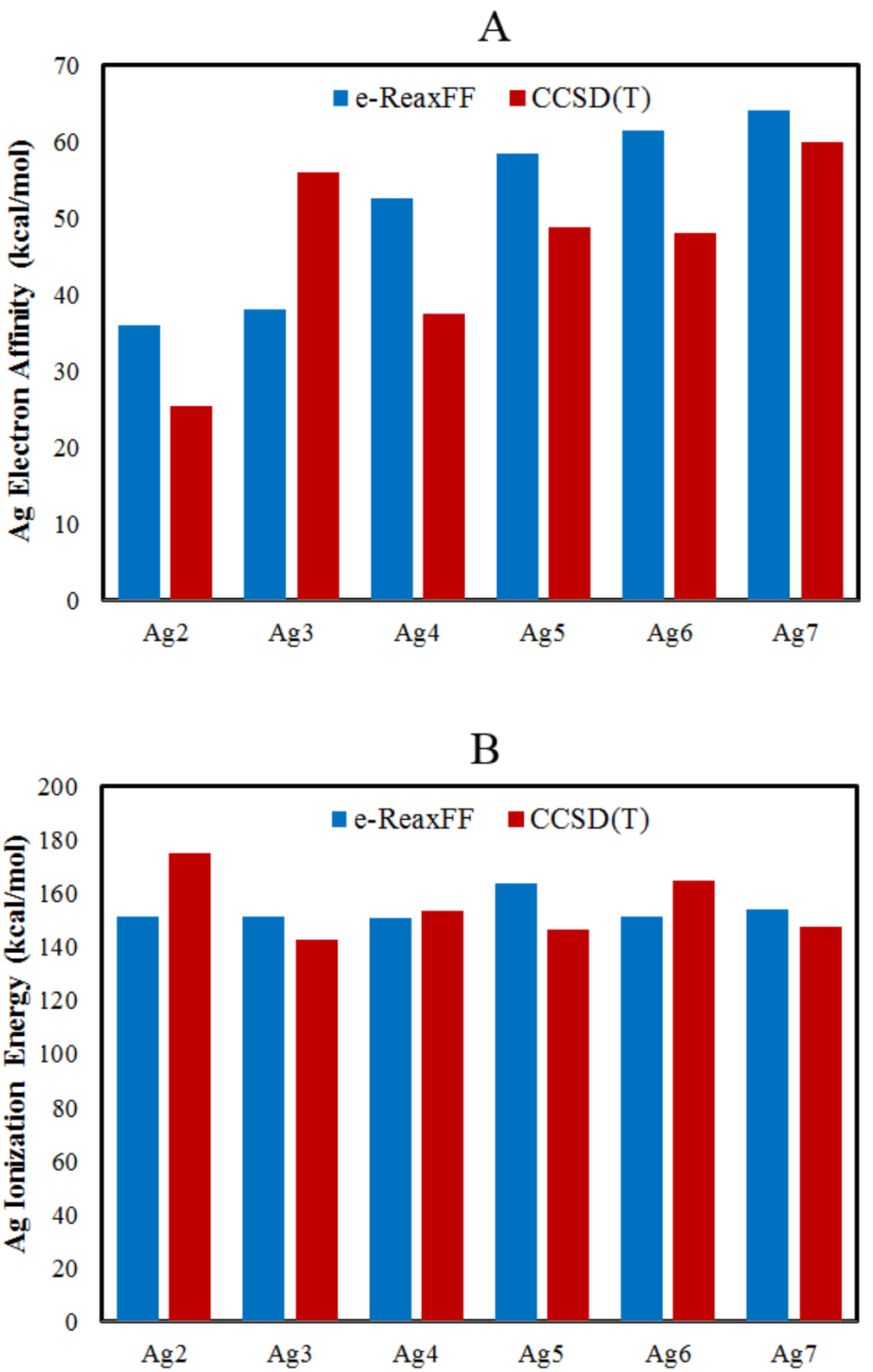

Figure 6. Electron affinities (A) and ionization energies (B) for Ag_2-Ag_7 taken from CCSD(T)

calculations by Duanmu *et al.*[16]

Figure 6 contains the ionization energy (IE) and electron affinity (EA) of every cluster size sampled by Duanmu *et al.*[16]. e-ReaxFF currently struggles to reproduce the EAs of the Ag clusters in our data set, but does well with reproducing IEs. Nevertheless, e-ReaxFF does correctly predict that every Ag cluster in our dataset will release significant amounts of energy when accepting an electron and the prediction for the amount of energy improves with increasing cluster size. Coupled with the good predictions for IEs, we believe that e-ReaxFF can be used for modelling redox reactions involving Ag clusters in MD simulations.

Ag_4 isomerization simulations

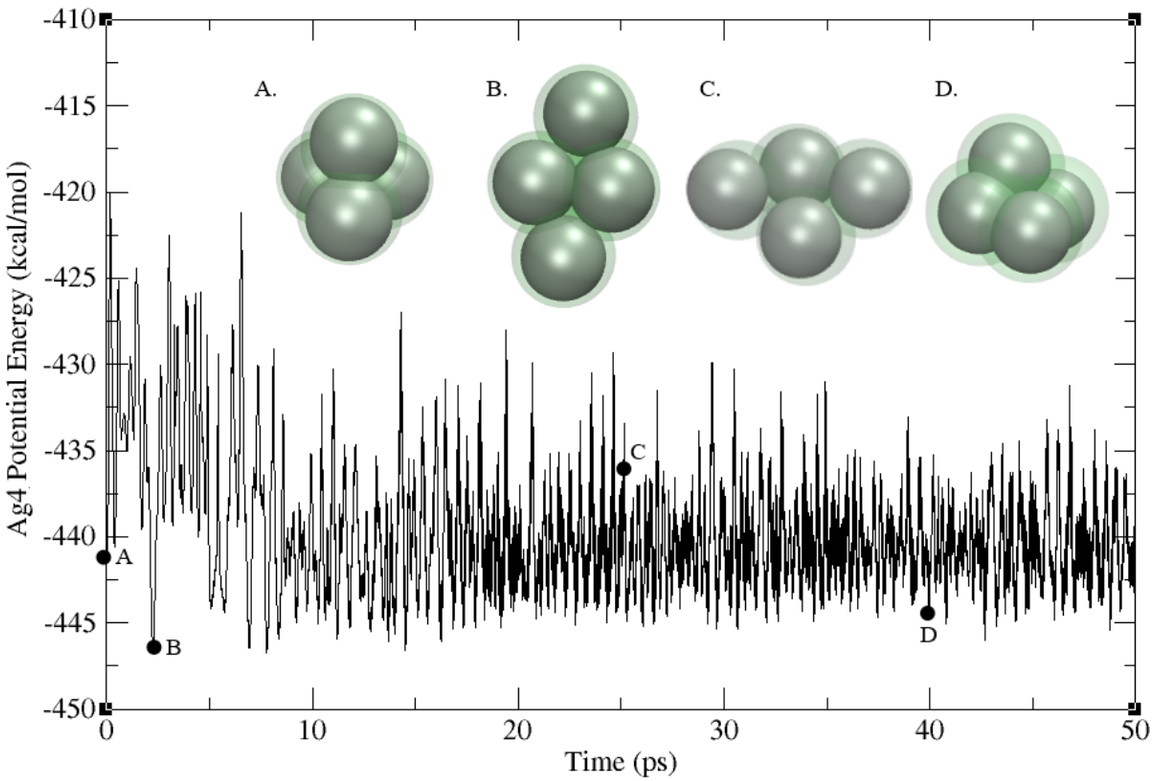

Figure 7. Potential energy as a function of time from an MD simulation of Ag_4 at T = 300 K, along with snapshots of various observed clusters.

Figure 7 shows the total potential energy during an MD simulation beginning with a 3D, tetrahedral Ag4_2 cluster at T = 300 K. The 3D Ag4_2 structure (Fig. 7A) readily converts into planar structures (Fig. 7B and 7C). *Ab initio* calculations for Ag_4 predict a structure nearly identical to the 2D structure seen in 7B. e-ReaxFF is able to attain this structure in a remarkably short amount of time because it both eliminates the non-zero-dihedral energetic penalty and maximizes the number of bonds for a 2D structure. Other, less stable geometries observed included variations of different, under-coordinated 2D structures as well as 3D structures (Fig. 7D).

Ag_5 isomerization simulations

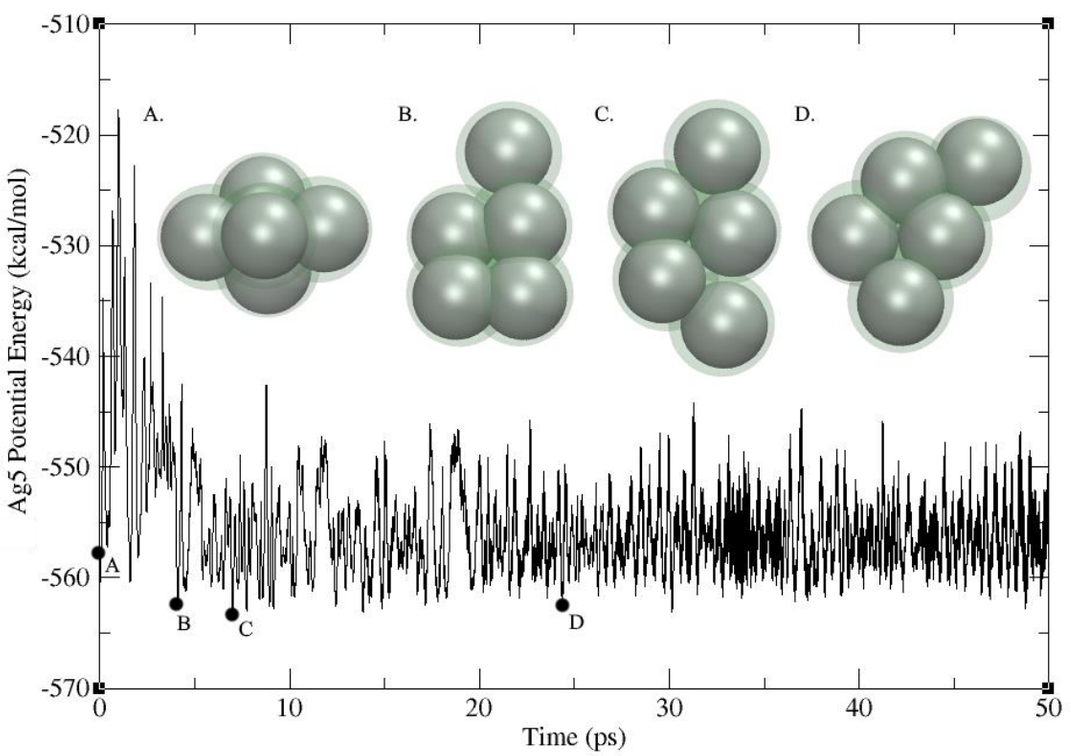

Figure 8. The potential energy as a function of time from an MD simulation of Ag_5 at T = 300 K, along with snapshots of various observed clusters.

Figure 8 shows the total potential energy from an MD simulation of an Ag_5 cluster at T = 300 K. Here, we see that a 2D geometry is preferred. The 3D Ag5_4 cluster (Fig. 8A) is unstable at moderate temperatures and readily converts to the 2D Ag5_1 structure (Fig. 8B) during the simulation. Also observed are 2D structures with defects (Fig. 8C and 8D), causing them to be higher in energy than Ag5_1. Higher-energy structures include highly under-coordinated Ag_5 chains as well as other 3D structures.

Ag_6 isomerization simulations

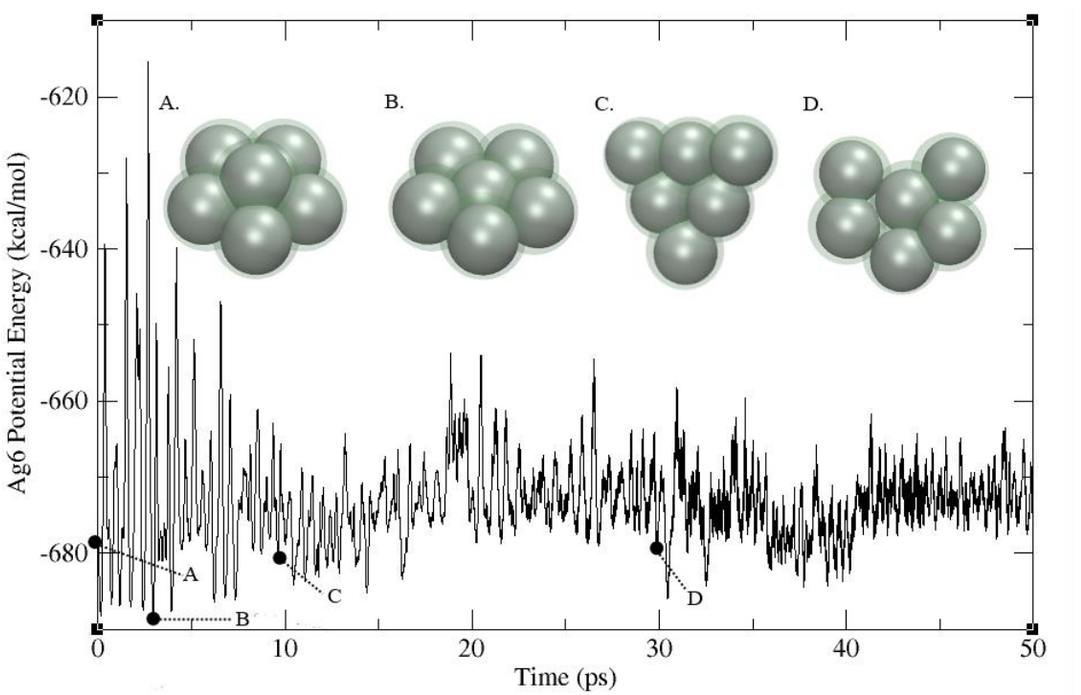

Figure 9. Potential energy as a function of time from an MD simulation of Ag_6 at T = 300 K, along with snapshots of various observed clusters.

Figure 9 shows the potential energy from an MD simulation of Ag_6 at 300 K. The simulations begin with the 3D Ag6_2 structure (A), which rapidly flattens out into the 2D Ag6_3 (B). Other sampled structures are 2D and include distortions of Ag6_1 (C) and Ag6_4 (D).

Ag_7 isomerization simulations

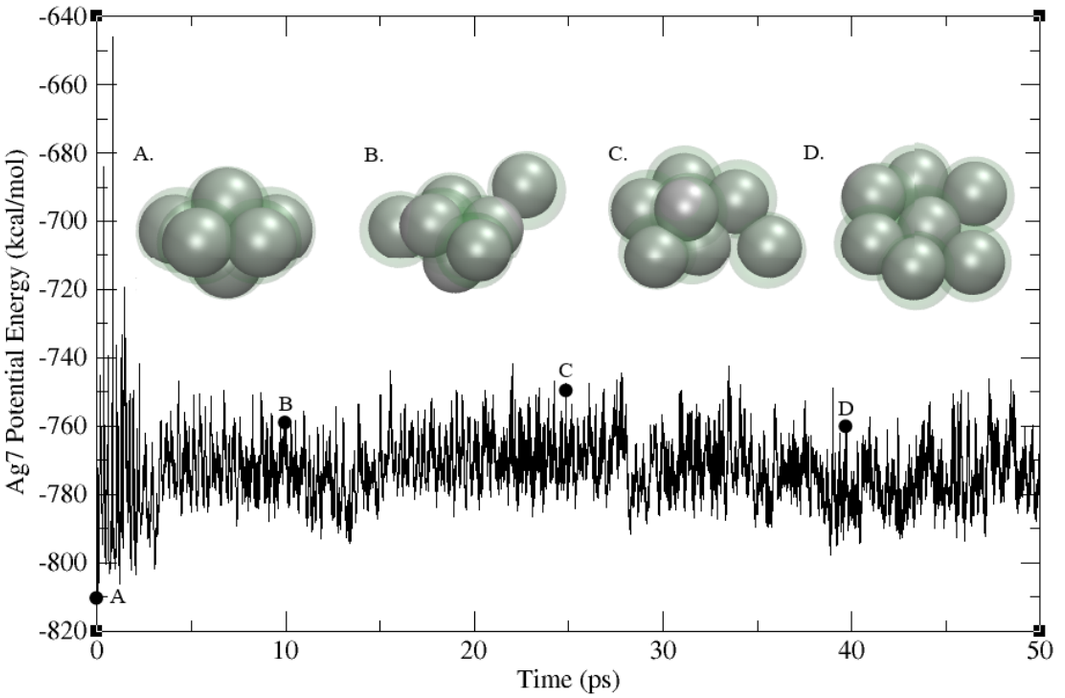

Figure 10. Potential energy as a function of time from an MD simulation of Ag_7 at T = 700 K, along with snapshots of various observed clusters.

Figure 10 shows the potential energy from an MD simulation beginning with the most-stable Ag_7 isomer at T = 700 K. From the initial Ag7_1 structure (Fig. 10A), the sampled structures from the first 25 ps of the simulation involve perturbations of the atoms in the central ring of the Ag7_1 cluster (Fig. 10B and C). Ag_7 is the smallest cluster in our data set that is 3D and resists flattening into a 2D structure at higher temperatures, unlike the smaller clusters. Approximately half-way through the simulation, the cluster converts from 3D to 2D but remains significantly higher in energy than the initial 3D structure.

Ag_{25} folding simulations

Figure 11 shows the total potential energy from an MD simulation of an Ag_{25} sheet at 500 K. The 2D Ag_{25} sheet (Fig. 11A) is unstable at moderate temperatures and readily converts to the 3D Ag_{25} structure (Fig. 11E). The planar cluster undergoes in-plane rearrangements of the Ag atoms, as well as the formation of chains and branches extending from the main section of the sheet (Fig. 11B and 11C). After the first atoms break the 2D plane (Fig. 11D), the structure readily undergoes 2D to 3D conversion.

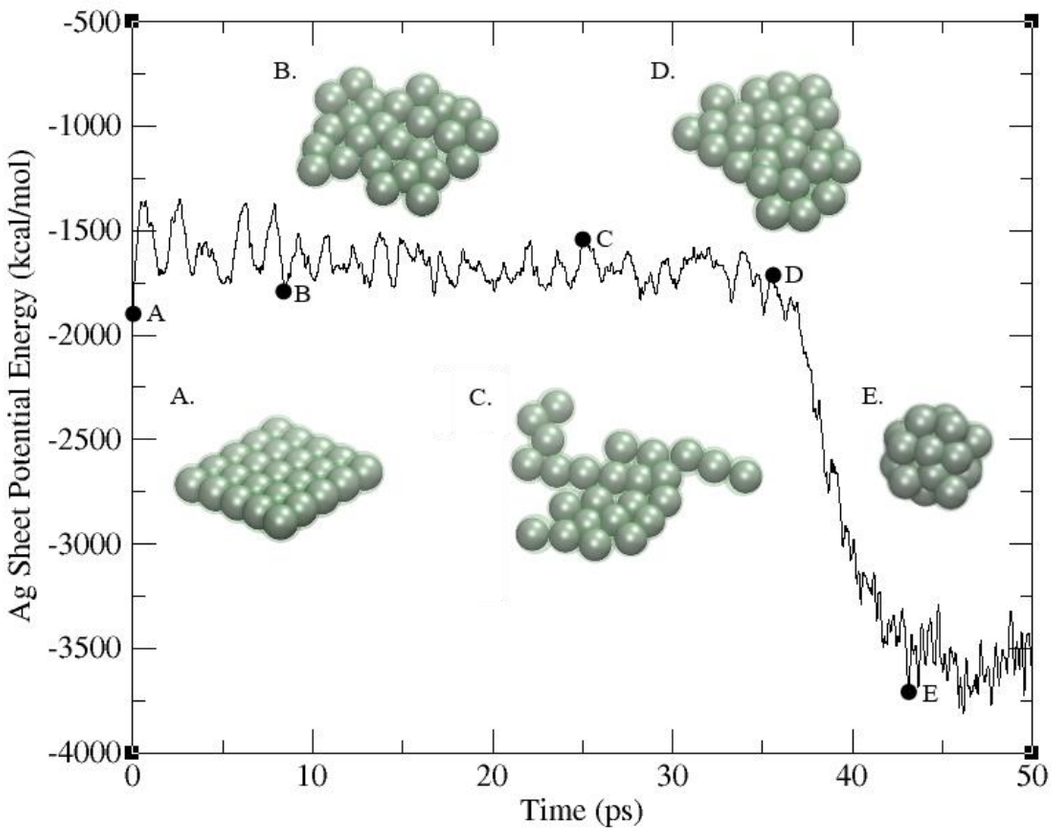

Figure 11. Snapshots taken from an MD simulation of a 2D Ag_{25} sheet at T = 500 K. The simulations begin with the planar Ag_{25} structure (A) which sees plenty of in-plane movement of its atoms (B and C) before the 2D plane is broken (D) and the cluster rapidly collapses into a 3D Ag_{25} cluster (E).

AgCl Reduction Simulations

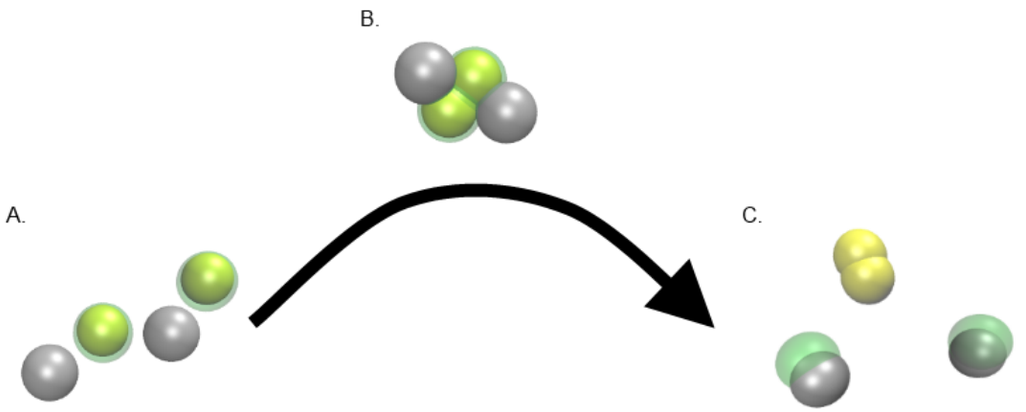

Figure 12. Reduction mechanism of 2AgCl at elevated temperatures observed using e-ReaxFF. Two sets of AgCl pairs align with one another (A) before the chlorines (yellow spheres) aggregate to form Cl_2 (B). Simultaneously, the excess electrons (green spheres) are transferred from the Cl_2 molecule to the Ag^+ ions (silver spheres) yielding 2 Ag^0 atoms.

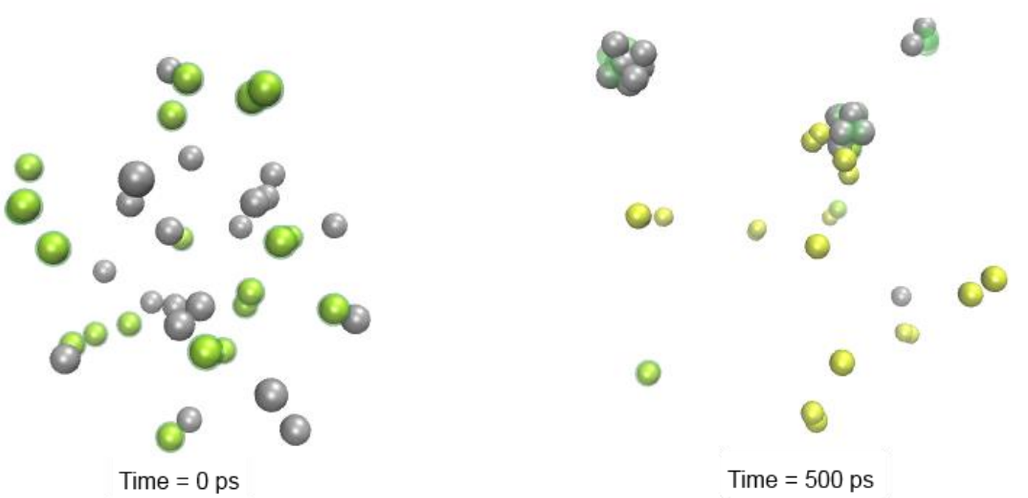

Figure 13. Initial and final conditions in an MD simulation containing 20 Ag^+ and 20 Cl^- ions at 450 K. The chloride ions are described by a neutral chlorine atom (yellow sphere) paired with an electron (green sphere). Chloride ions spontaneously reduce silver cations (silver spheres) to form Cl_2 and Ag^0. The silver atoms then aggregate to form clusters.

Above, we showed that our e-ReaxFF potential can correctly model the lowest-energy isomer Ag nanocluster of various sizes. To demonstrate that it can capitalize on the explicit electronic degree of freedom present in e-ReaxFF, we simulated a system of 20 Ag^+ cations and 20 Cl^- anions at 450 K. The Cl portion of this potential was parameterized to only reproduce the electron affinity, ionization energy, and enthalpy of formation of Cl and Cl_2 respectively. Cl^- was chosen because of its experimental relevance. Typically, silver halide reduction is a photo-induced event or occurs in the presence of an explicitly added reducing agent, neither of which is present in these simulations.[43,44] However, the density of the simulated system is low enough that Cl^- ions can interact with Ag^+ ions in relative isolation and avoid clustering together to form an AgCl lattice. These simulations are intended to only demonstrate that electrons may be transferred in a realistic fashion using e-ReaxFF and are not intended to be conclusive of any actual silver halide reaction or growth mechanisms for these reasons.

Figure 12 shows a reduction event between a pair of Ag^+ cations (silver spheres) and Cl^- ions (yellow with green spheres). The AgCl pairs initially orient themselves such that the equivalent charges are separated by their counter-ions (Fig. 12 A) before the Cl^- ions aggregate and form a Cl-Cl bond (Fig. 12 B). The Cl_2 molecule forms and simultaneously donates its excess electrons (green spheres) to the Ag^+ ions yielding Ag^0 atoms (Fig. 12 C). This process occurred multiple times in the MD simulation described above and after 500 ps, three Ag clusters had formed (Fig. 13).

Plasmon oscillation simulations

Noble metal nanoparticles exhibit a collective oscillation of their conduction electrons in response to an oscillating electromagnetic field which is commonly referred to as surface plasmon resonance or simply plasmon resonance.[45] e-ReaxFF and its explicit electronic degrees

of freedom can potentially model the effects of plasmon resonance. This can be done by placing a nanoparticle between positive and negative charges in order to polarize the particle by pushing all of the electrons toward the positive charge before removing both charges and allowing the electrons to begin oscillating freely. Figure 14 shows an example of such a simulation using a Ag_{55} cluster as an example.

An electronically relaxed Ag_{55} cluster was placed between one +5 and one -5 point charge in canonical ensemble MD simulations at T = 10 K with a 0.250 fs timestep for 25 ps and using the velocity-Verlet time-integration algorithm with the Berendsen thermostat. This simulation was unstable using a Nose-Hoover thermostat – as such we switched to the more robust, but physically less correct, Berendsen thermostat. This instability when using a Nose-Hoover thermostat can be traced to the highly exothermic nature of this simulation which consequently leads to atoms with very high velocities that are better handled by the velocity-rescaling algorithm in the Berendsen thermostat.[46] This permitted the electrons to migrate toward the positively charged side of the cluster without disturbing the heavier Ag atoms significantly. The point charges were then removed and further MD simulations at T = 300 K were conducted to monitor the position of the electron cloud's center of mass. Two masses for the electrons were compared, 1.0 amu and 5.0 amu, to demonstrate the effects of our significantly heavier explicit electrons on the plasmon frequency.

Figure 14 shows the *x*-coordinate, *i.e.* the coordinate along the polarization vector, of the electron cloud's center of mass for a polarized Ag_{55} cluster with electrons weighing 1 amu and 5 amu. Upon removal of the charges maintaining polarization, the COM rapidly moved in the opposite direction of polarization and began resonating. The 1.0 amu electron oscillated with a wavelength of ~7500 nm and the 5.0 amu electron resonated at ~22.5 μm. The 5 amu electron

cloud displays a more uniform oscillation than the 1 amu electrons, but with a predictably lower frequency. Neither plasmon oscillated with a frequency in the established visible/UV region[1,47] with both e-ReaxFF plasmon oscillation frequencies being in the IR range. This is most likely the result of the heavier electrons and can be alleviated by reducing their mass – although this will invoke a decrease in the size of the required timestep. Nevertheless, these simulations do demonstrate that plasmon oscillation can, in principle, be simulated using an e-ReaxFF description of a metal nanoparticle.

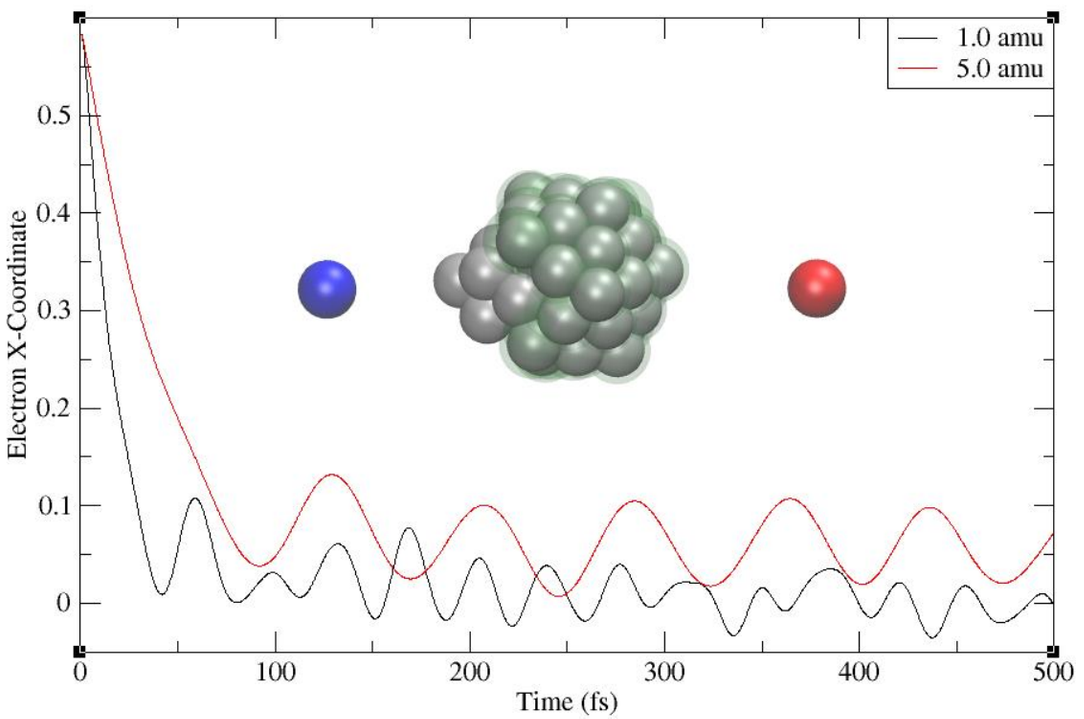

Figure 14. Initially polarized structure of Ag_{55} positioned between positive (red sphere) and negative (blue sphere) charges with the position of the electron cloud center of mass (COM) in the *x*-direction during an MD simulation at T = 300 K. Upon removal of the charges maintaining polarization, the COM rapidly moved in the opposite direction of polarization and began resonating with the 1.0 amu electrons oscillating with a wavelength of ~7500 nm and the 5.0 amu electrons at ~22.5 μm.

Conclusions

In this work, we parameterized an e-ReaxFF description of silver nanoparticles that reproduces a 2D geometry preference at small cluster sizes ($N < 7$ atoms) and a 3D geometry preference at all other cluster sizes. This was possible by introducing a four-body torsional term into the potential that dominates at the small cluster sizes while being overpowered by the two-body bonding term at larger sizes. Our potential is capable of modelling the 2D to 3D transition from small to larger clusters, as well as simulating the growth of nanoclusters from a metal salt and plasmon oscillations in Ag nanoclusters. These capabilities are encouraging and, with further development, should enable us to model more complex phenomena, such as cluster aggregation and the impact of reduction rates on cluster morphology.

Supplementary Material

See the supplementary material for the Cartesian coordinates of all reference structures and the contents of the reactive force field file.

Available Software

The standalone e-ReaxFF code used to perform the force field parameterization and the MD simulations reported in this article can be obtained following a request to the Material Computation Center website at Penn State (https://www.mri.psu.edu/materials-computation-center/connect-mcc).

Acknowledgements

We acknowledge support and training provided by the Computational Materials Education and Training (CoMET) NSF Research Traineeship (grant number DGE-1449785). Simulations in this work were conducted in part with Advanced Cyberinfrastructure computational resources provided by the Institute for Cyber Science at the Pennsylvania State University (https://ics.psu.edu/).

Data Availability Statement

The data that supports the findings of this study are available within the article and its supplementary material.

References

[1] E. Ringe, J.M. McMahon, K. Sohn, C. Cobley, Y. Xia, J. Huang, G.C. Schatz, L.D. Marks, and R.P. Van Duyne, J. Phys. Chem. C **114**, 12511 (2010).

[2] Y. Zhou, W.A. Saidi, and K.A. Fichthorn, J. Phys. Chem. C **118**, 3366 (2014).

[3] A.T. Fafarman, S.H. Hong, S.J. Oh, H. Caglayan, X. Ye, B.T. Diroll, N. Engheta, C.B. Murray, and C.R. Kagan, ACS Nano **8**, 2746 (2014).

[4] K.J. Lee, B.H. Jun, T.H. Kim, and J. Joung, Nanotechnology **17**, 2424 (2006).

[5] T.S. Rodrigues, M. Zhao, T.H. Yang, K.D. Gilroy, A.G.M. da Silva, P.H.C. Camargo, and Y. Xia, Chem. - A Eur. J. **24**, 16944 (2018).

[6] S.H. Lee and B.H. Jun, Int. J. Mol. Sci. **20**, (2019).

[7] V. Kravets, Z. Almemar, K. Jiang, K. Culhane, R. Machado, G. Hagen, A. Kotko, I. Dmytruk,

K. Spendier, and A. Pinchuk, Nanoscale Res. Lett. **11**, (2016).

[8] X.Y. Dong, Z.-W. Gao, K.F. Yang, W.-Q. Zhang, and L.-W. Xu, Catal. Sci. Technol. **5**, 2554 (2015).

[9] Z.-J. Jiang, C.-Y. Liu, and L.-W. Sun, J. Phys. Chem. B **109**, 1730 (2005).

[10] J.J. Polte, CrystEngComm **17**, 6809 (2015).

[11] N.T.K. Thanh, N. Maclean, and S. Mahiddine, Chem. Rev. **114**, 7610 (2014).

[12] M. Wuithschick, B. Paul, R. Bienert, A. Sarfraz, U. Vainio, M. Sztucki, R. Kraehnert, P. Strasser, K. Rademann, F. Emmerling, and J. Polte, Chem. Mater. **25**, 4679 (2013).

[13] X. Qi, T. Balankura, and K.A. Fichthorn, J. Phys. Chem. C **122**, 18785 (2018).

[14] M. Itoh, V. Kumar, T. Adschiri, and Y. Kawazoe, J. Chem. Phys. **131**, 174510 (2009).

[15] B.B. Dale, R.D. Senanayake, and C.M. Aikens, APL Mater. **5**, (2017).

[16] K. Duanmu and D.G. Truhlar, J. Phys. Chem. C **119**, 9617 (2015).

[17] S. Lecoultre, A. Rydlo, J. Buttet, C. Félix, S. Gilb, and W. Harbich, J. Chem. Phys. **134**, 184504 (2011).

[18] T.L. Haslett, K.A. Bosnick, and M. Moskovits, J. Chem. Phys. **108**, 3453 (1998).

[19] F. Wang, V.N. Richards, S.P. Shields, and W.E. Buhro, Chem. Mater. **26**, 5 (2014).

[20] P. Sutter, Y. Li, C. Argyropoulos, and E. Sutter, J. Am. Chem. Soc. **139**, 6771 (2017).

[21] A.C.T. Van Duin, S. Dasgupta, F. Lorant, and W.A. Goddard, J. Phys. Chem. A **105**, 9396

(2001).

[22] M. Raju, S.-Y. Kim, A.C.T. Van Duin, and K.A. Fichthorn, J. Phys. Chem. C **117**, 10558 (2013).

[23] J. Ludwig, D.G. Vlachos, A.C.T. Van Duin, and W.A. Goddard, J. Phys. Chem. B **110**, 4274 (2006).

[24] K. Chenoweth, A.C.T. Van Duin, and W.A. Goddard, J. Phys. Chem. A **112**, 1040 (2008).

[25] C.L. Chia, C. Avendaño, F.R. Siperstein, and S. Filip, Langmuir **33**, 11257 (2017).

[26] L. Huang, K.E. Gubbins, L. Li, and X. Lu, Langmuir **30**, 14832 (2014).

[27] M. Aryanpour, A.C.T. Van Duin, and J.D. Kubicki, J. Phys. Chem. A **114**, 6298 (2010).

[28] M.M. Islam, G. Kolesov, T. Verstraelen, E. Kaxiras, and A.C.T. Van Duin, J. Chem. Theory Comput. **12**, 3463 (2016).

[29] T. Verstraelen, P.W. Ayers, V. Van Speybroeck, and M. Waroquier, J. Chem. Phys. **138**, 074108 (2013).

[30] W.J. Mortier, S.K. Ghosh, and S. Shankar, J. Am. Chem. Soc. **108**, 4315 (1986).

[31] R. Peverati and D.G. Truhlar, J. Chem. Theory Comput. **8**, 2310 (2012).

[32] M. Chen, J.E. Dyer, K. Li, and D.A. Dixon, J. Phys. Chem. A **117**, 8298 (2013).

[33] Axel D. Becke, J. Chem. Phys. **98**, 5648 (1993).

[34] L. Chengteh, Y. Weitao, and R.G. Parr, Phys. Rev. B **37**, 785 (1988).

[35] D. Figgen, K.A. Peterson, M. Dolg, and H. Stoll, J. Chem. Phys. **130**, (2009).

[36] S.Y. Kim, N. Kumar, P. Persson, J. Sofo, A.C.T. Van Duin, and J.D. Kubicki, Langmuir **29**, 7838 (2013).

[37] S.N. Korobeynikov, V. V. Alyokhin, and A. V. Babichev, Acta Mech. **229**, 2343 (2018).

[38] P. Pyykkö, Annu. Rev. Phys. Chem. **63**, 45 (2012).

[39] X.J. Kuang, X.Q. Wang, and G. Bin Liu, J. Mol. Model. **17**, 2005 (2011).

[40] W. Huang and L.S. Wang, Phys. Rev. Lett. **102**, 3 (2009).

[41] J. Yang, Q. Zhang, L. Chen, G. Wang, and X. Chen, Adv. Sci. **3**, 1 (2016).

[42] P.L. Williams, Y. Mishin, and J.C. Hamilton, Model. Simul. Mater. Sci. Eng. **14**, 817 (2006).

[43] A. Król-Gracz, E. Michalak, P.M. Nowak, and A. Dyonizy, Cent. Eur. J. Chem. **9**, 982 (2011).

[44] T.H. James and G. Korxfeld, Chem. Rev. **30**, 1 (1942).

[45] V.G. Kravets, A. V. Kabashin, W.L. Barnes, and A.N. Grigorenko, Chem. Rev. **118**, 5912 (2018).

[46] B.D. Jensen, K.E. Wise, and G.M. Odegard, J. Comput. Chem. **36**, 1587 (2015).

[47] C. An, S. Wang, Y. Sun, Q. Zhang, J. Zhang, C. Wang, and J. Fang, J. Mater. Chem. A **4**, 4336 (2016).

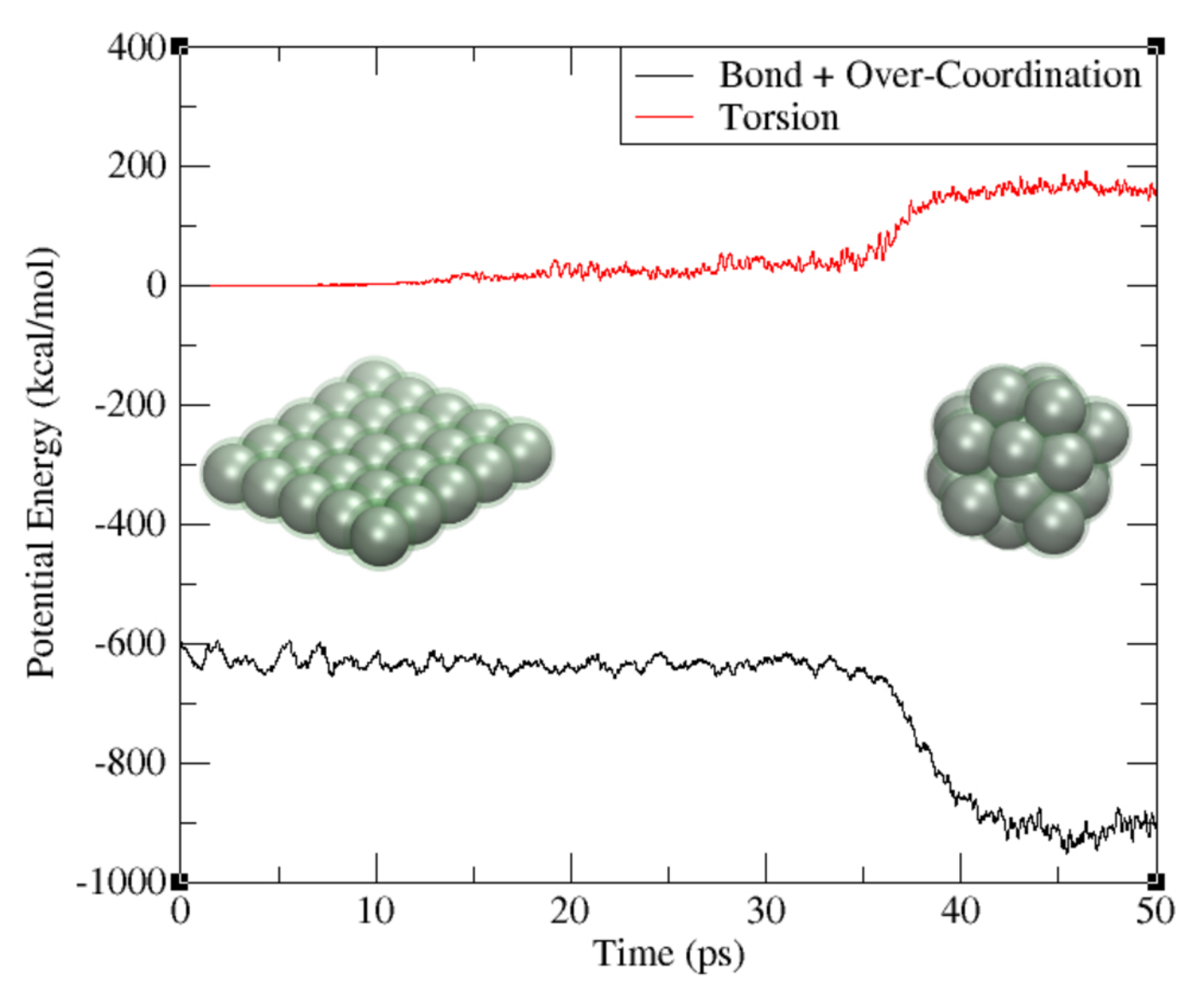
Bond + Over-Coordination
Torsion
Potential Energy (kcal/mol)
400
200
0
-200
-400
-600
-800
-1000
0
10
20
30
40
50
Time (ps)

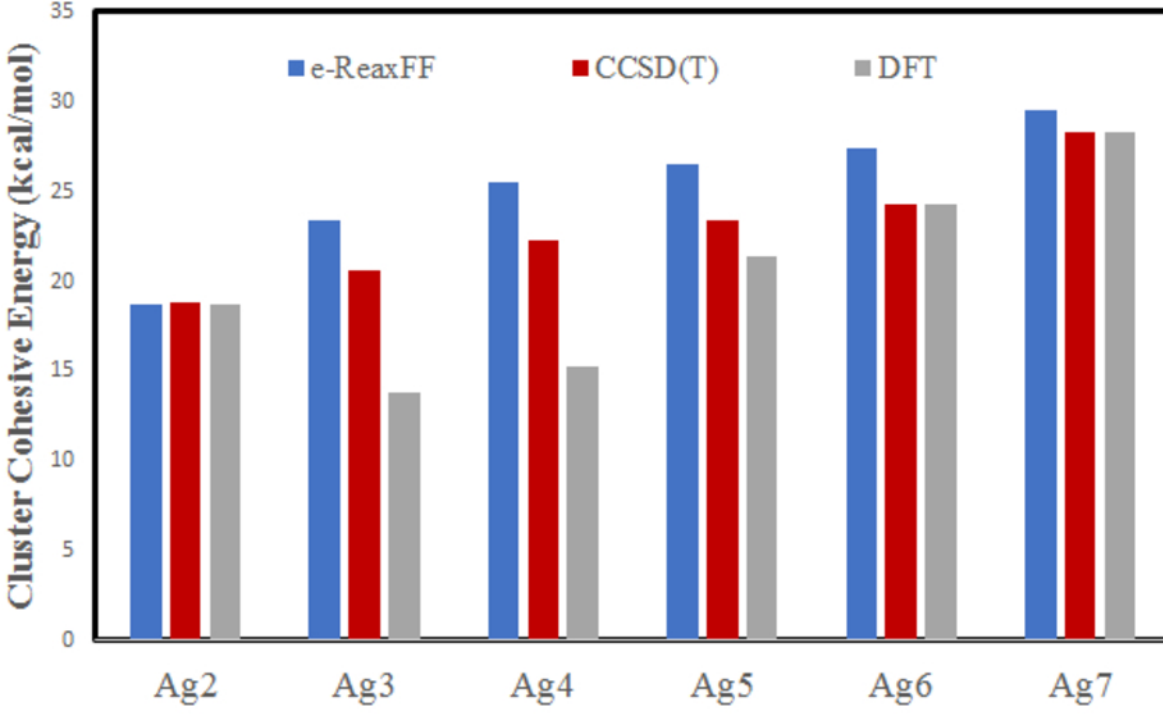
e-ReaxFF
CCSD(T)
DFT
Cluster Cohesive Energy (kcal/mol)
35
30
25
20
15
10
5
0
Ag2
Ag3
Ag4
Ag5
Ag6
Ag7

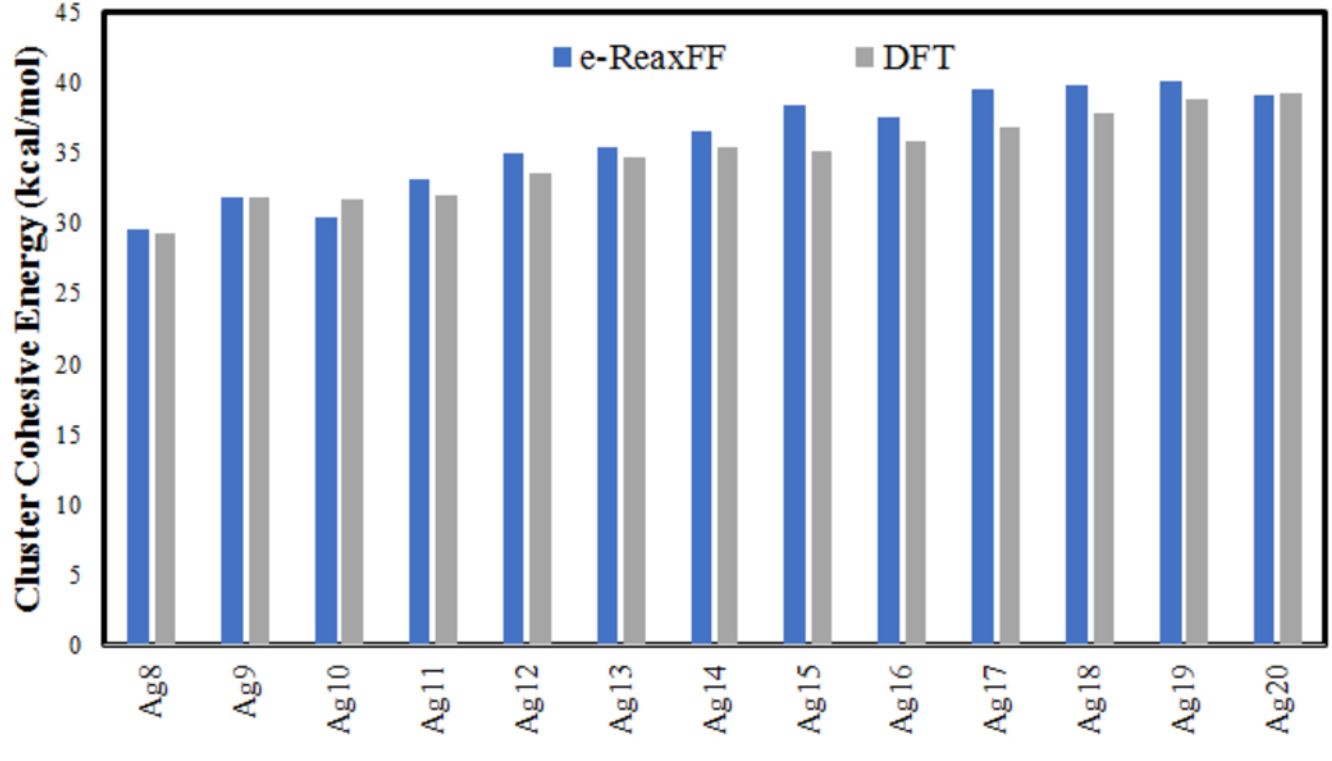
Cluster Cohesive Energy (kcal/mol)
45
40
35
30
25
20
15
10
5
0
e-ReaxFF
DFT
Ag8
Ag9
Ag10
Ag11
Ag12
Ag13
Ag14
Ag15
Ag16
Ag17
Ag18
Ag19
Ag20

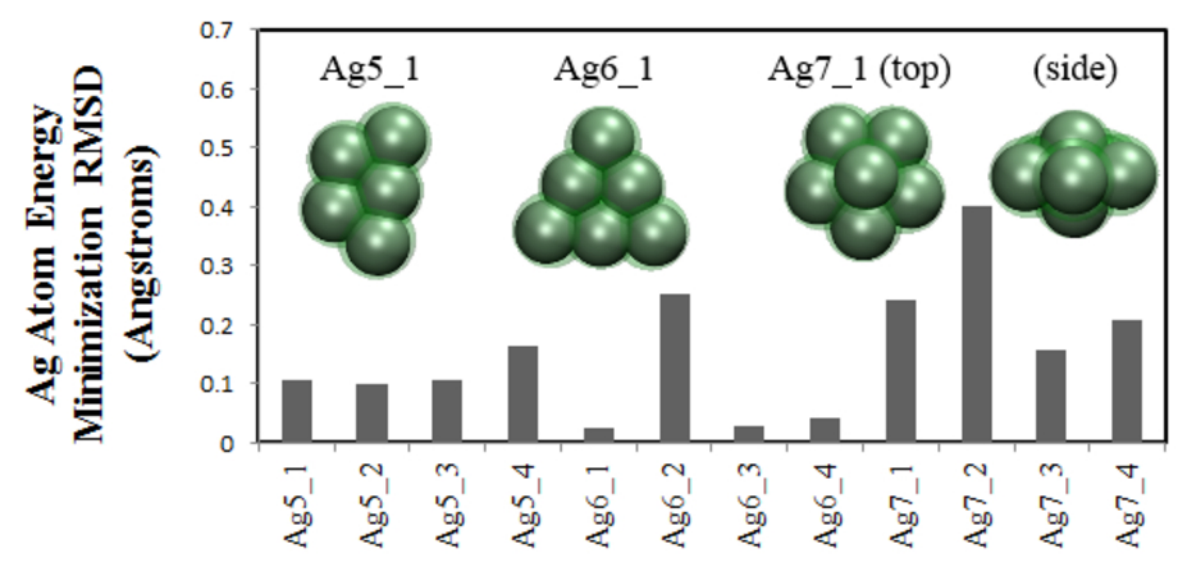
Ag Atom Energy Minimization RMSD (Angstroms)
0.7
0.6
0.5
0.4
0.3
0.2
0.1
0
Ag5_1
Ag6_1
Ag7_1 (top)
(side)
Ag5_1
Ag5_2
Ag5_3
Ag5_4
Ag6_1
Ag6_2
Ag6_3
Ag6_4
Ag7_1
Ag7_2
Ag7_3
Ag7_4

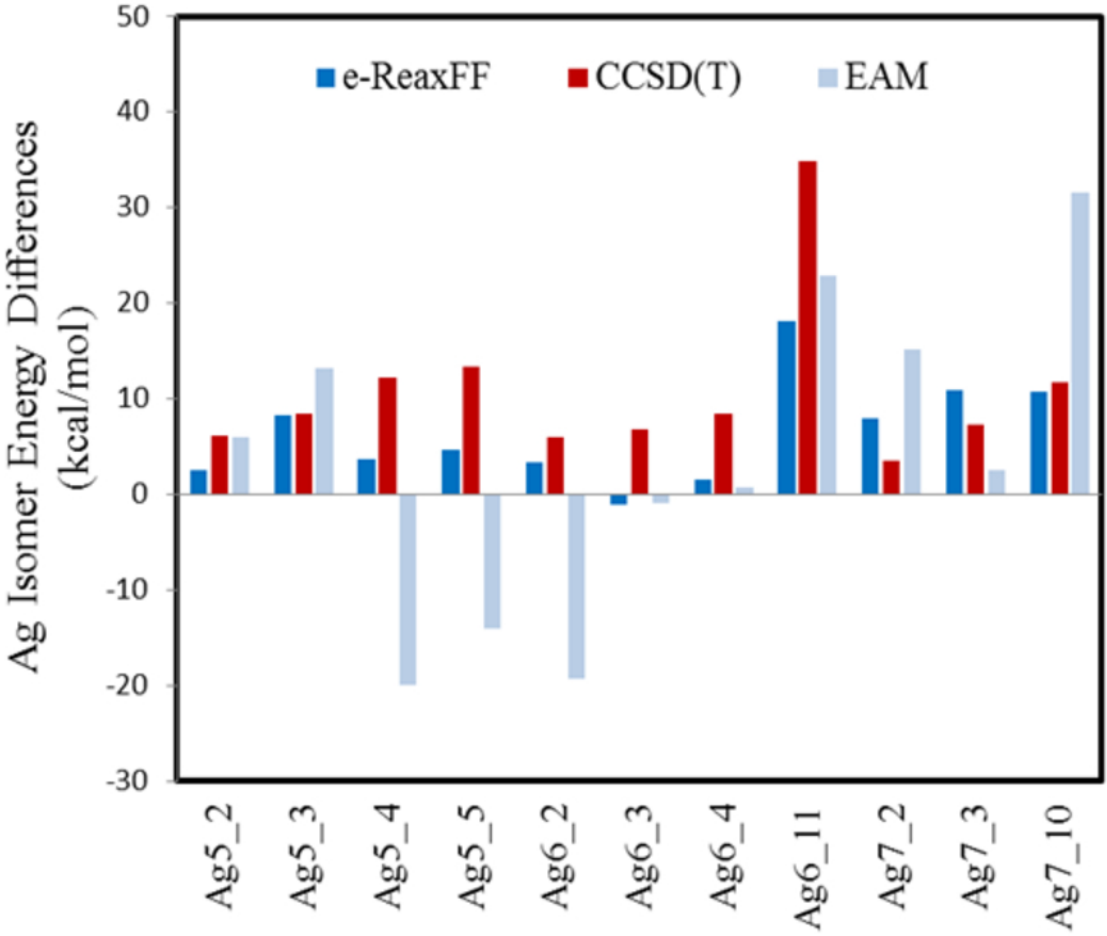
e-ReaxFF
CCSD(T)
EAM
Ag Isomer Energy Differences (kcal/mol)
50
40
30
20
10
0
-10
-20
-30
Ag5_2
Ag5_3
Ag5_4
Ag5_5
Ag6_2
Ag6_3
Ag6_4
Ag6_11
Ag7_2
Ag7_3
Ag7_10

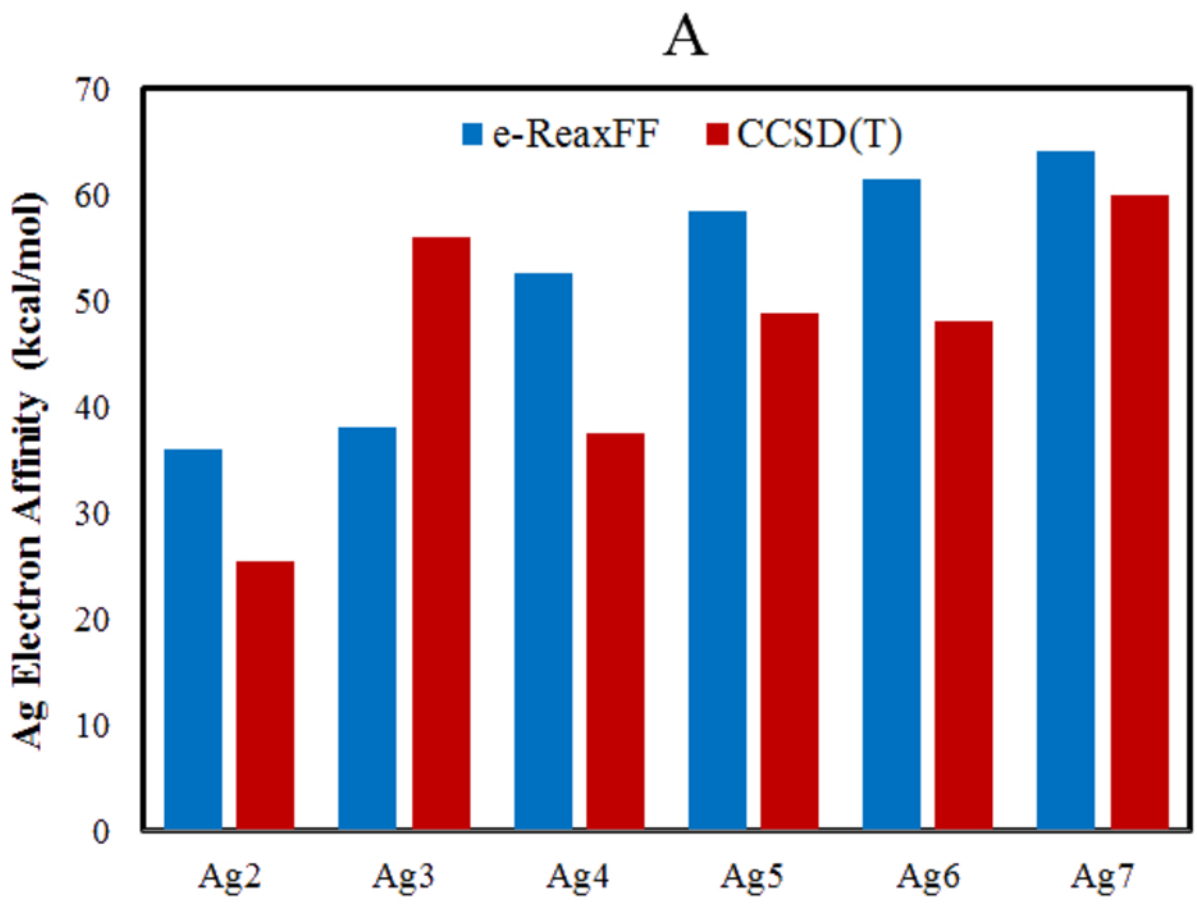
A
e-ReaxFF
CCSD(T)
Ag Electron Affinity (kcal/mol)
70
60
50
40
30
20
10
0
Ag2
Ag3
Ag4
Ag5
Ag6
Ag7

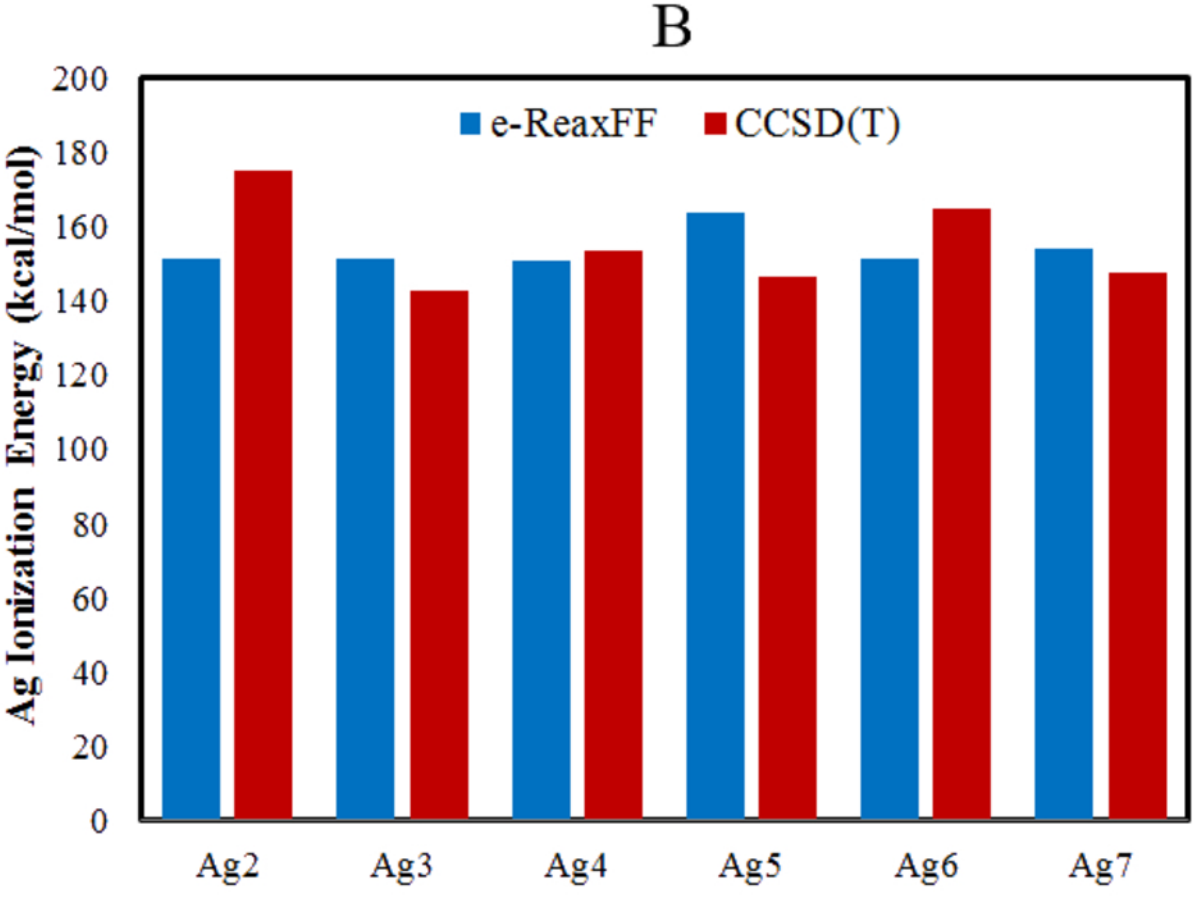
B
e-ReaxFF
CCSD(T)
Ag Ionization Energy (kcal/mol)
200
180
160
140
120
100
80
60
40
20
0
Ag2
Ag3
Ag4
Ag5
Ag6
Ag7

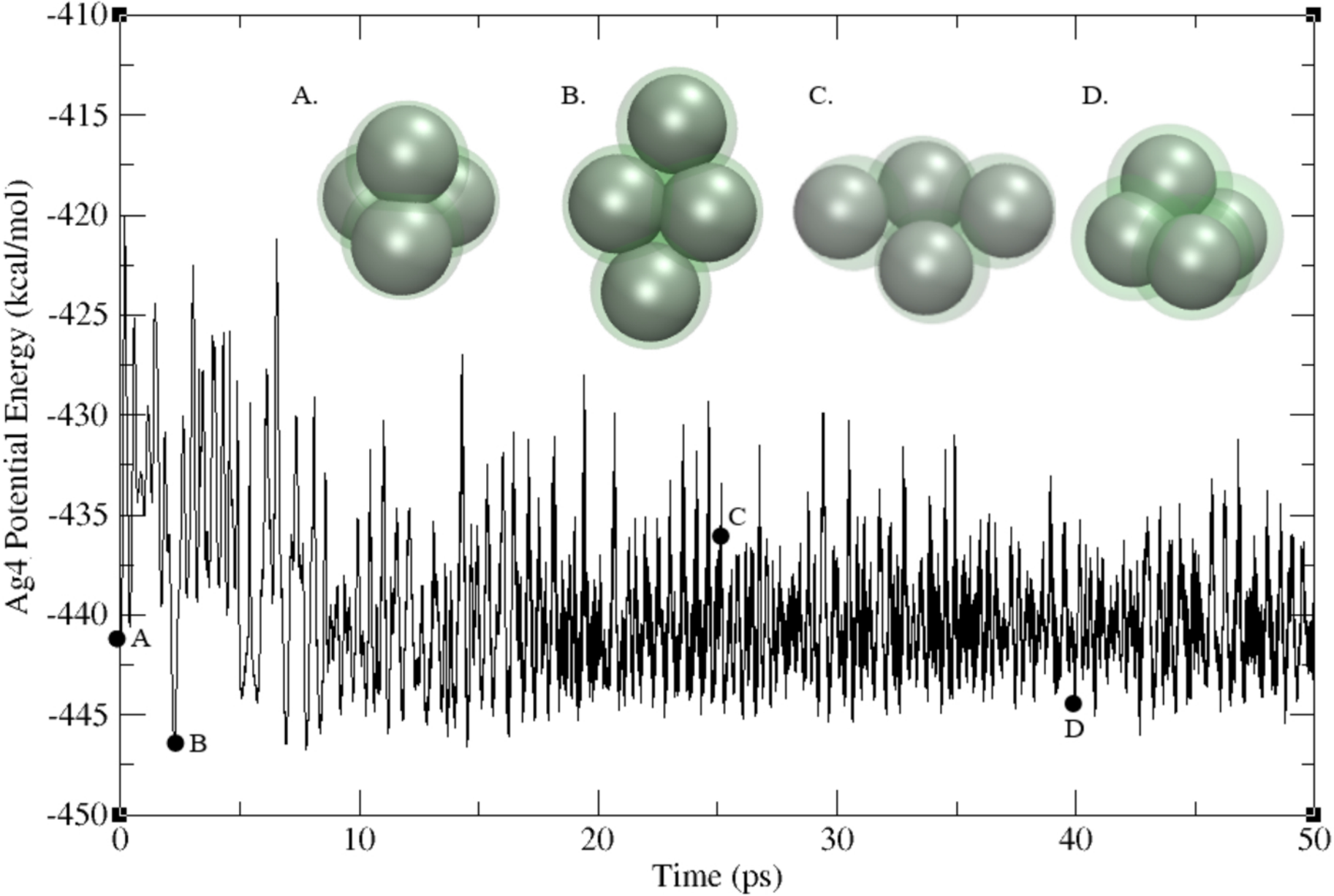
A.
B.
C.
D.
-410
-415
-420
-425
-430
-435
-440
-445
-450
Ag4 Potential Energy (kcal/mol)
A
B
C
D
0
10
20
30
40
50
Time (ps)

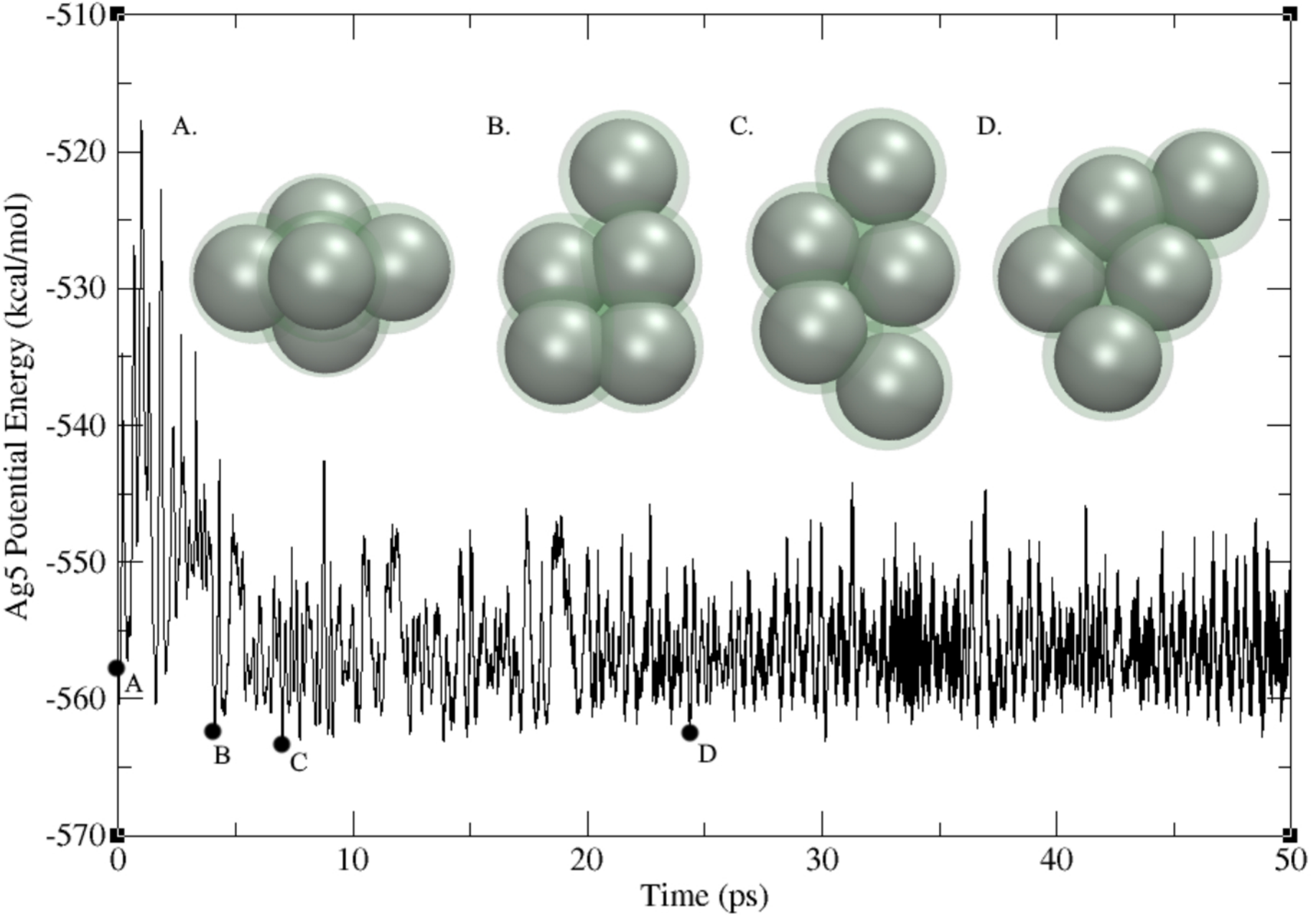
A.
B.
C.
D.
-510
-520
-530
-540
-550
-560
-570
Ag5 Potential Energy (kcal/mol)
A
B
C
D
0
10
20
30
40
50
Time (ps)

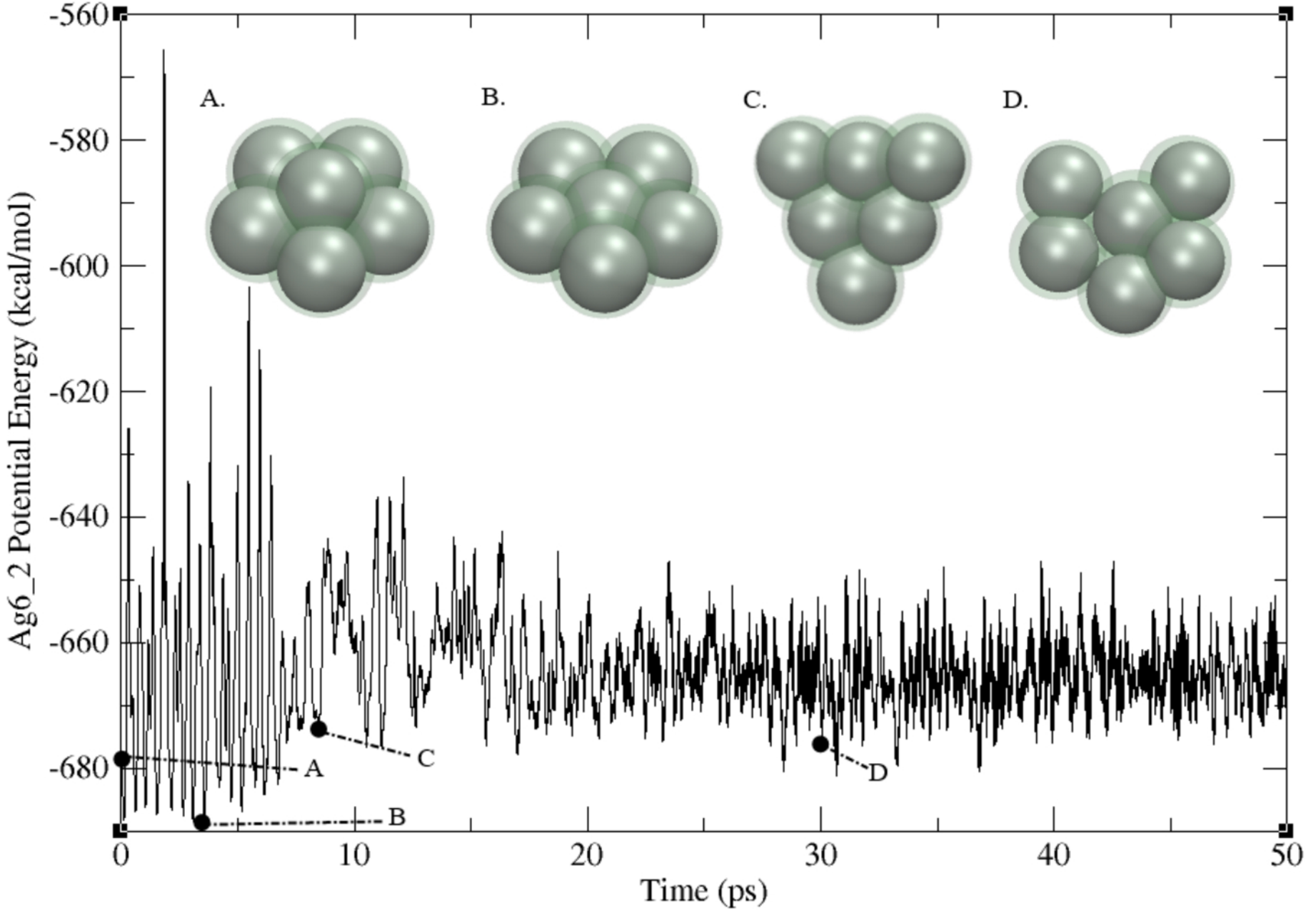
A.
B.
C.
D.
-560
-580
-600
-620
-640
-660
-680
Ag6_2 Potential Energy (kcal/mol)
A
B
C
D
0
10
20
30
40
50
Time (ps)

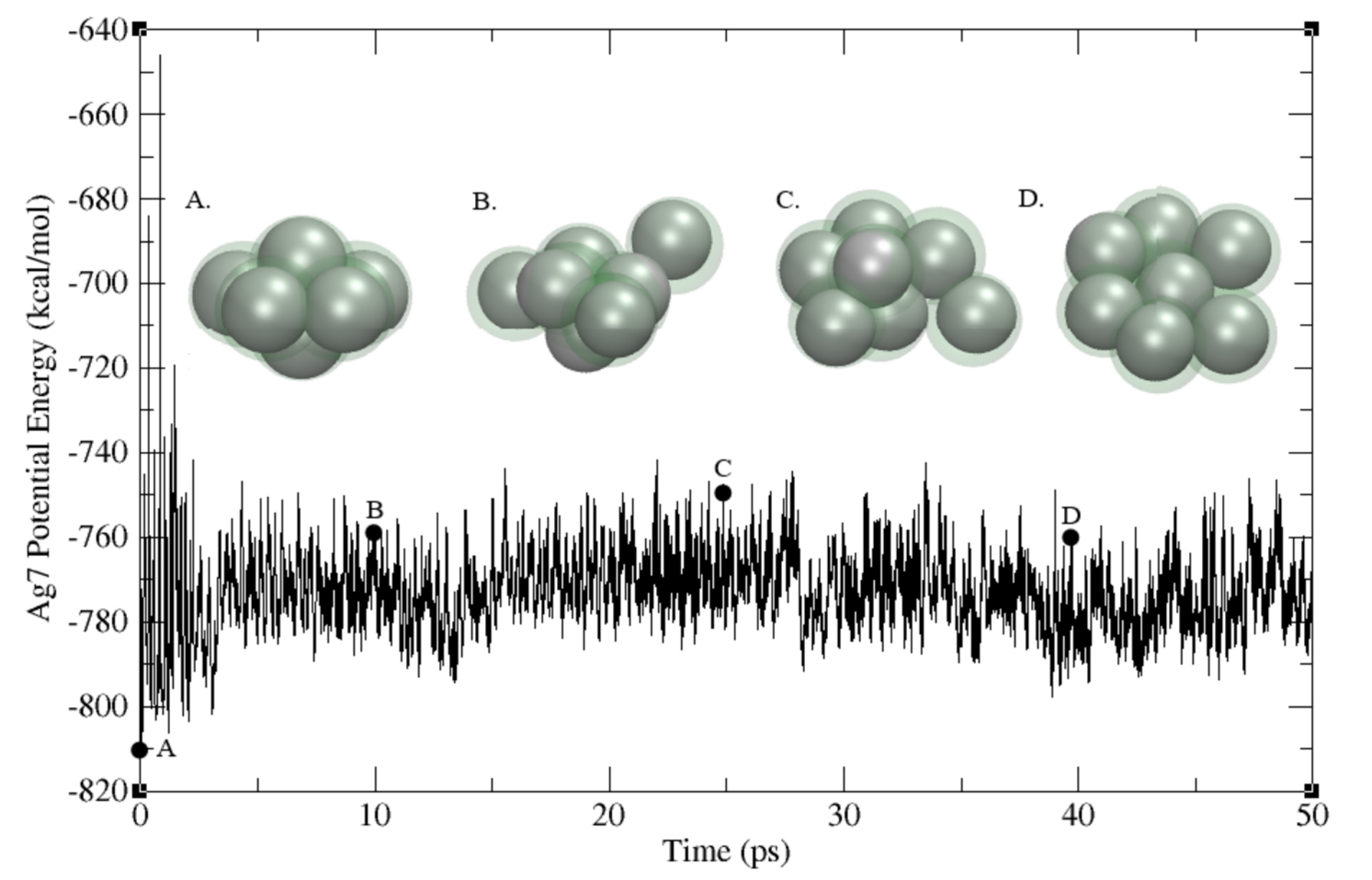
-640
-660
-680
-700
-720
-740
-760
-780
-800
-820
Ag7 Potential Energy (kcal/mol)
0
10
20
30
40
50
Time (ps)
A.
B.
C.
D.
A
B
C
D

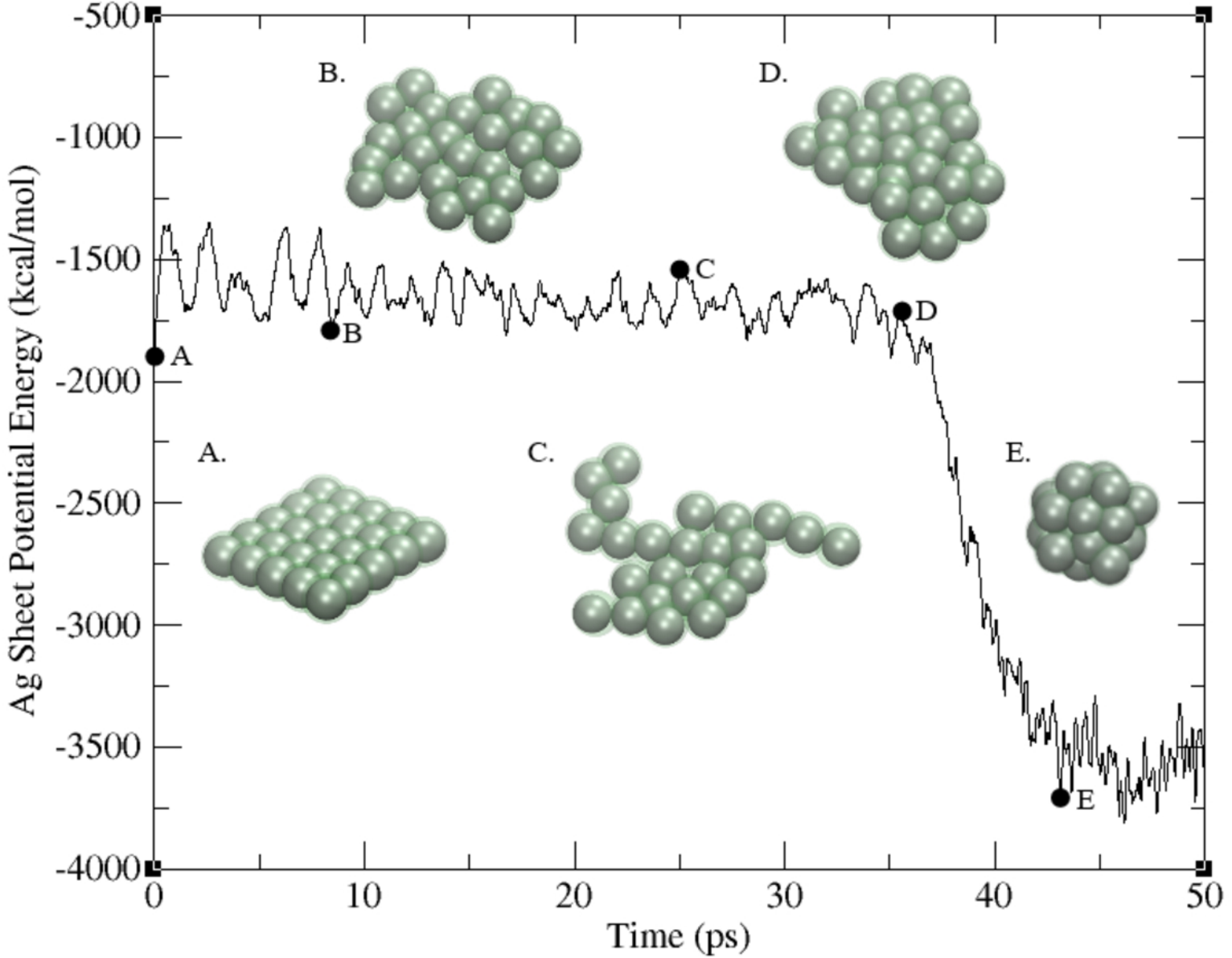
-500
-1000
-1500
-2000
-2500
-3000
-3500
-4000
0
10
20
30
40
50
Time (ps)
Ag Sheet Potential Energy (kcal/mol)
A
B
C
D
E
A.
B.
C.
D.
E.

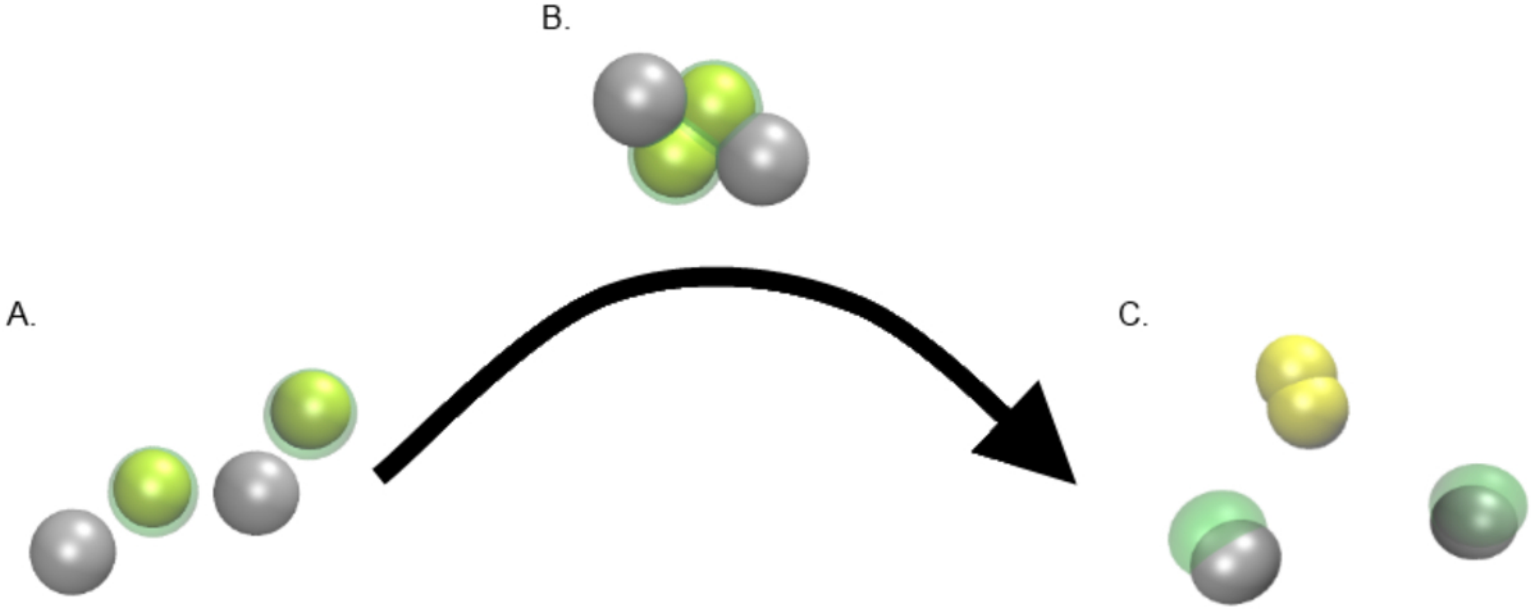
B.
A.
C.

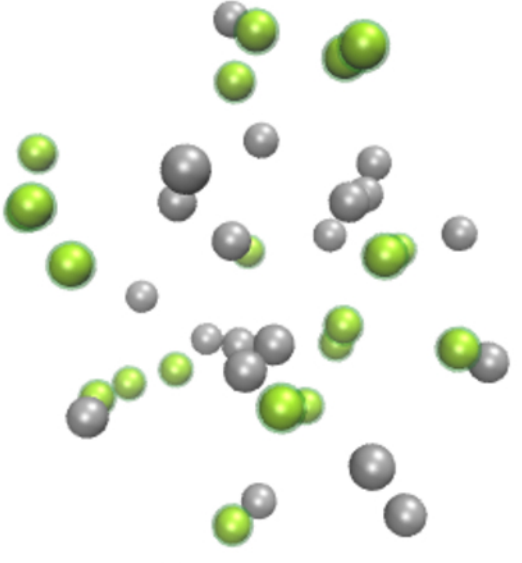

Time = 0 ps

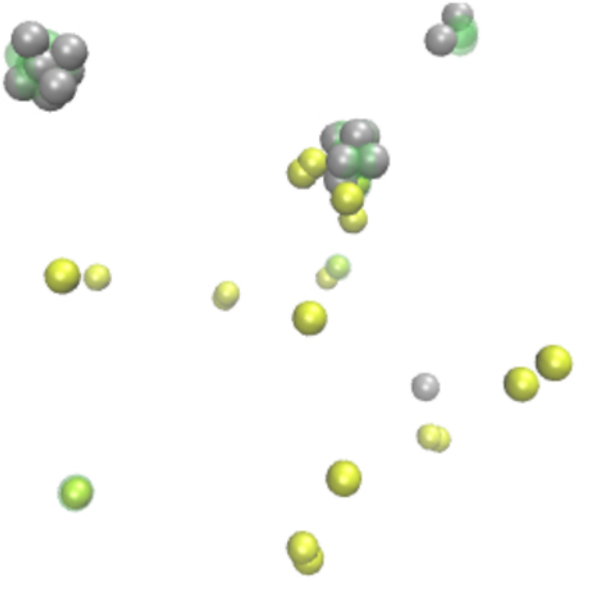

Time = 500 ps

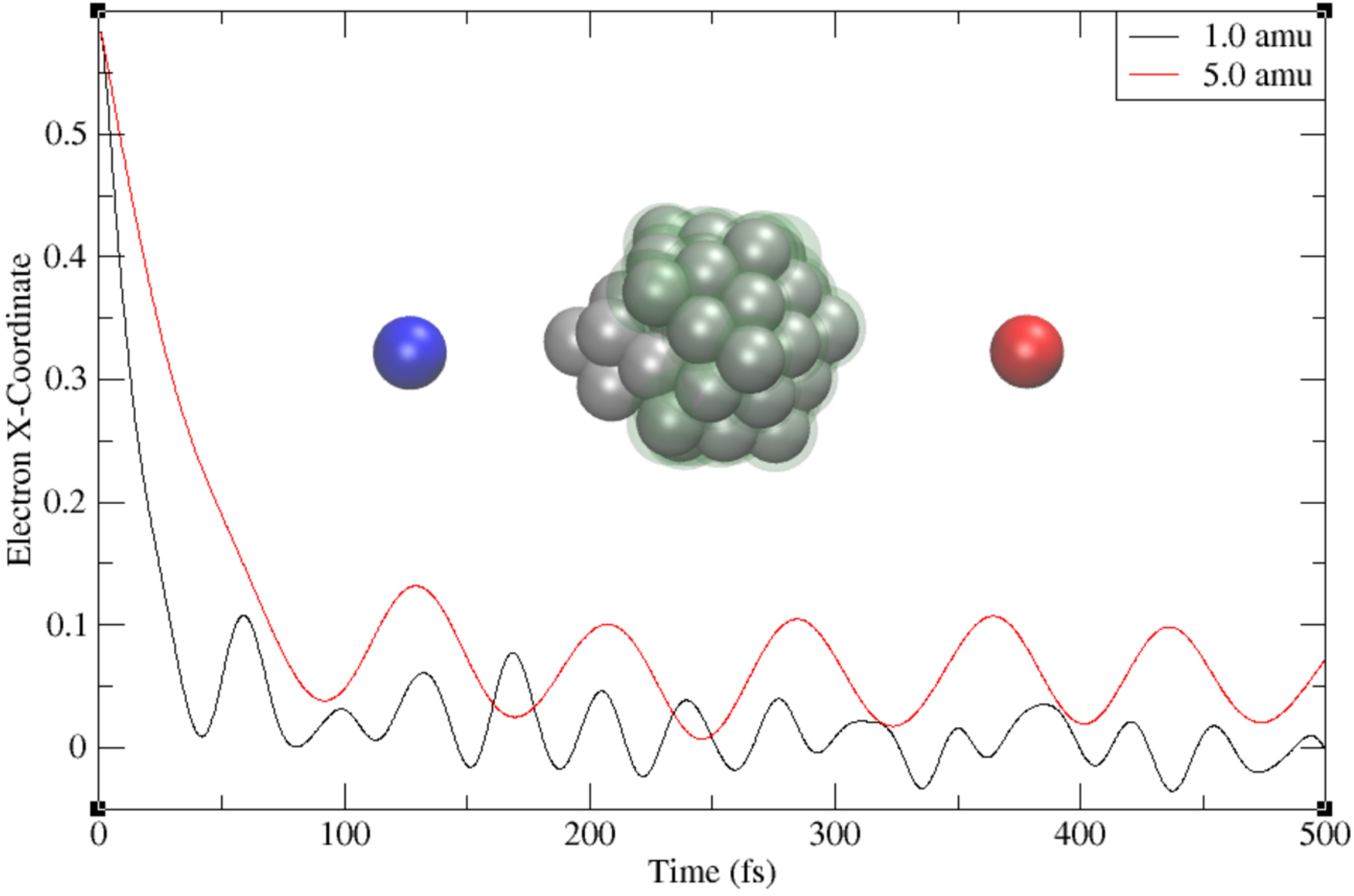
1.0 amu
5.0 amu
Electron X-Coordinate
0.5
0.4
0.3
0.2
0.1
0
0
100
200
300
400
500
Time (fs)